Energy Yield Model for Bifacial PV Systems: A study and analysis of temperature & rear irradiance models.

Master Thesis Report

By

RAJA SUNDEEP REDDY GALI

in partial fulfilment of the requirements for the degree of

Master of Science
in Sustainable Energy Technology

At Energy Research Centre of Netherlands (ECN)

TU Delft Supervisor:	Prof. Dr. Arthur Weeber
Company Supervisor:	Dr. Gaby J.M. Janssen
Examiners:	Dr. O. Isabella
	Dr. A. Rodrigo Mor

Date: 21-11-2017

TU Delft
Delft University of Technology

ECN
Energy research Centre of the Netherlands

Abstract

In order to make the bifacial yield prediction models commercially available, a lot of work their development, improvement and validation is being done by many research institutes. At Energy research center of the Netherlands (ECN), one such model is under development. In this project, couple of aspects were investigated to give better insight into improving the model. The two main aspects of the model that were investigated were the rear irradiance estimation and the temperature prediction of the model.

Analysis of rear irradiance aspect of the bifacial yield model through simulations at low tilt angles and elevations should in practice result low rear irradiance but the results showed the opposite. From the literature, a new factor called acceptance was implemented in the rear irradiance model which led to correction in estimation of rear irradiance. For the temperature model, initially indoor measurements of three laminates of bifacial cells and three laminates of monofacial cells were performed under solar simulator. The experiment resulted in finding differences in measured and cell temperatures for all six laminates. According to measured temperatures, the bifacial cell laminates were hotter than their monofacial counterparts, which may not be correct due to higher absorption of irradiance by backsheets in bifacial cell laminates. The differences in calculated cell temperature and measured temperature were investigated and were found to be different. The heating behavior of all laminates was modelled and heat capacity and heat transfer coefficient found through modelling were found to be in good agreement with literature values. Outdoor measurements were used for temperature analysis of bifacial panels and again the differences in calculated cell temperature and measured temperature were found. Non-steady state temperature model was found to be more accurate for low resolution meteorological and insolation data of less than ten minutes as compared to the steady state model used by current ECN model. The difference between measured and cell temperature was translated in terms of heat transfer coefficient and for this difference, the annual energy yield results showed a variation of 1.45 %.

The results of the project showed improvement of the bifacial yield model by ECN through an improved rear irradiance estimation. Furthermore, non-steady model should be used in case the input meteorological and insolation data is in less than ten-minute interval.

Acknowledgement

Firstly, I would like to thank Dr. Gaby Janssen for giving me this opportunity to work on my master thesis at ECN. I would like to thank Dr. Gaby Janssen for her tireless help, patient advice and proficient advice during the research. I am grateful for her feedbacks and input on the thesis work during the past ten months. Her joyous nature and positive attitude have constantly kept me upbeat and confident. It was just an amazing experience working at ECN under the supervision of Dr. Gaby Janssen. I would also like to convey my gratefulness to Dr. Bas van Aken for his help and mentorship in certain aspects of the research. I have learnt a lot from both of you.

I would like to thank my TU Delft supervisor, Dr. Arthur Weeber for introducing ECN to me and due to which I was able to do this project. I want to give my sincere thanks for your patience you showed with me and this project. Also, I would like to give my deepest gratitude for organizing the presentations at the PVMD group. Furthermore, I would like to thank the PVMD group for giving me an opportunity to present my research halfway through it and for the comments which have helped me in better preparation of presentations.

I would like to thank Koen de Groot and Mark Jansen of ECN for helping me understand working of certain measurement equipment crucial to my research. I would also like to thank the Jong ECN group for organizing various social events which helped in providing certain relief and positivity and also led to me making many international friends. I would also like thank my friends at ECN for making my time at ECN very enjoyable and positive.

Furthermore, I would like to give my greatest appreciation to my two best friends Ebrar and Rithwick for giving me great memories in the last two years and for your support, friendship and inspiring me to achieve my goals during my two years at TU Delft. I would also like to give my gratitude to my former high school teacher Mamata for inspiring me to take this path in renewable energy. Finally, and most importantly, I would like to give my greatest gratitude and appreciation to my parents. Without their support, I would not be here in this position in my life.

Table of Contents

List of Figures

List of Symbols

G_M	Total irradiance incident on a solar panel.
G_R	Total irradiance on the rear surface of the bifacial solar panel.
G_b	Horizontal direct irradiance.
G_d	Horizontal diffuse irradiance.
A_i	Anisotropy index
$R_{b,rear}$	Ratio of beam irradiance on tilted surface (rear side of the panel) to the horizontal beam irradiance.
$f_{sh,rear}$	Factor for shading due to the panel behind.
$1 + f sin^3 \frac{\beta}{2}$	Horizon diffuse irradiance ($f-$ cloudiness factor).
ρ_g	Ground reflectance (albedo).
VF_f	View Factor with respect to the front side.
VF_r	View Factor with respect to the rear side.
β	Tilt angle.
$G_{R,refID}$	Ground reflected isotropic diffuse irradiance on rear side.
Acc_{ID}	Acceptance Factor for isotropic diffuse irradiance by the ground.
$G_{R,ref\ beam+CS}$	Ground reflected beam and circumsolar diffuse irradiance on rear side.
$Acc_{beam+CS}$	Acceptance Factor for beam and circumsolar diffuse irradiance by the ground.
H	Vertical length of the panel.
D	Pitch between two panels.
B	Elevation of the panel above ground.
X	Extra distance as seen by the rear side of panel due to elevated panels.
V_{go}	Ratio of semiconductor bandgap at 0 temperature (E_{go}) to electronic charge (q).
V_{oc}	Open circuit voltage.
γ_i	Temperature dependencies of parameters determining saturation current.
k	Thermal voltage.
T_m	Operating temperature of the solar module/cell.
I_{sc}	Short circuit current.
t	Thickness.
ρ	Density.
C_p	Specific heat capacity.
Q_{in}	Heat absorbed by the solar module.
h_c	Convective heat transfer.
T_a	Ambient temperature.
ϵ_f	Emissivity of the front surface.
ϵ_r	Emissivity of the rear surface.
T_{sky}	Sky temperature.
T_{ground}	Ground temperature.
σ	Boltzmann's constant.
U	Overall heat transfer coefficient.
$NOCT$	Normal operating cell temperature.
n	Ideality factor.

1 Introduction

The time is running out for humans to save what we have left of this wonderful planet. Renewable energy – two of most used words in recent times, seems to be the only option for the future energy consumption and hence growing and developing sustainably. Due to irreparable exploitation of natural resources like coal, oil and natural gas for energy consumption, the earth's climate has been gradually changing as it is known. Almost all the countries of UN have come together for the annual COP meeting in Paris in November, 2015 to discuss and set certain goals to mitigate the effect of climate change. One of the main goals is to keep the temperature from rising above 2 °C or less (from pre-industrial levels) and one of the main solution to achieve the target is to increase the share of renewables in the energy sector [1]. Though the renewables are growing steadily, to reach the goals of COP 21, the share of renewables has to increase rapidly. One such renewable energy is solar energy, which has the largest potential of all energy sources. Solar energy has a great potential to play a pivotal role in increasing the share of renewable energy in energy sector and in order compete with other sources with low prices like coal and fossil fuels, the costs have to reduce. Photovoltaics is a popular technology that uses the power of sun to generate electricity. The figure below shows the reduction of the costs of the PV technology globally from 2009 to 2015 and the prediction of the price reduction for the future given in [2]. Indicating that the low prices can accelerate the share of PV power in the electricity sector.

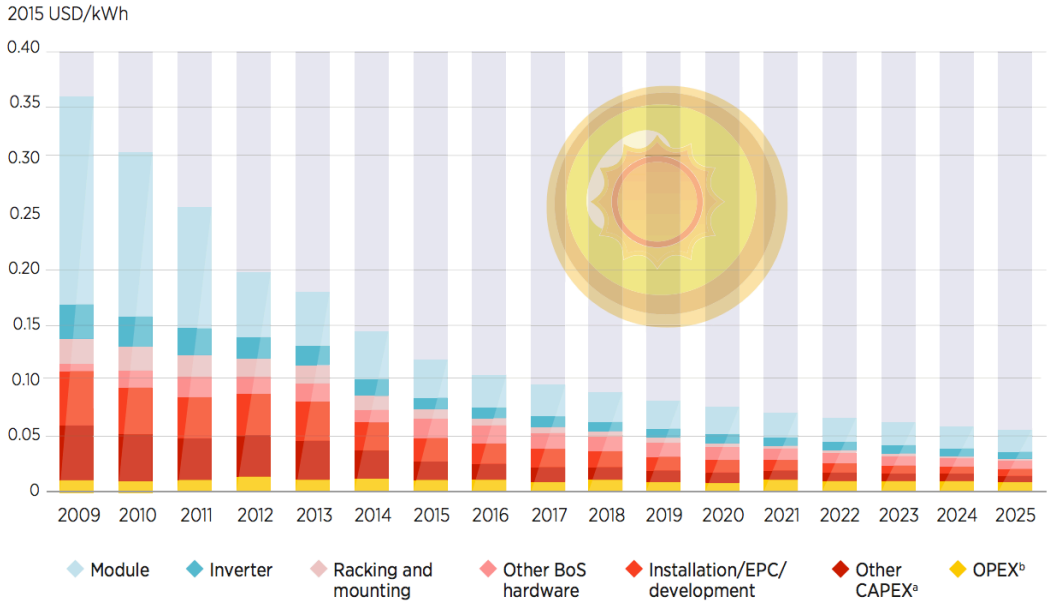

Figure 1.1 Reducing price of PV technology [2]

Obviously, the use of the solar energy in the energy sector can be increased by reducing the LCOE (Levelized Cost of Electricity). This can be done by either reducing the system costs or the increasing the energy output (increasing efficiency or optimisation of system) and also increasing the lifetime of the PV systems [3].

1.1 Bifacial PV technology

The bifacial solar cell technology has been studied since the 1960s but they have not caught attention until bifacial cells were fully developed. The working principle of the solar cell is it converts the incident irradiance falling on its surface directly into electrical energy. The bifacial solar cell technology utilizes the irradiance falling on both front and rear sides of the cell, and this is converted into electrical energy. As compared to the monofacial cell, its rear side in not fully metallized so as to allow light from the rear as seen in the figure 1.2 below. The irradiance reflected off the ground, results in more energy yield output as compared to the monofacial cell technology. The figure 1.2 below shows the structures of a typical monofacial and bifacial cells.

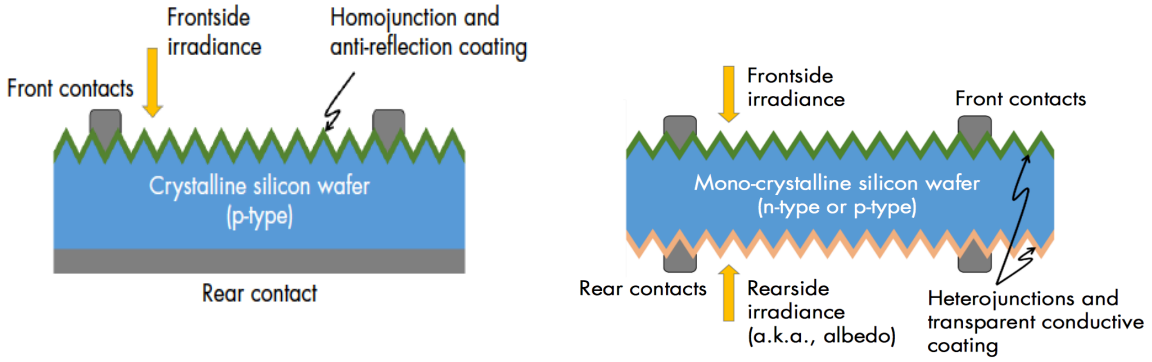

Figure 1.2. Structures of typical monofacial and bifacial cells. [3]

The term bifacial gain comes into picture here as it a common parameter that gives the amount of energy gained through the rear side in comparison to the front side. Another term important in the bifacial PV field is 'albedo'. It gives the fraction of light that would be reflected back from a ground surface. For example, a ground covered in concrete would give an albedo of ~0.2 [4]. There are different modules that use bifacial cells and most common bifacial technology is the bifacial module with transparent glass. There are other modules that have non-transparent backsheet instead of the transparent glass on the rear. This effectively becomes a monofacial module. The most common backsheets used are of white or black. This obviously limits the usage of rear irradiance but instead the light reflected off the backsheet would be used and therefore, white backsheet would be ideal.

1.2 Bifacial yield prediction models

Yield prediction models are necessary in order to simulate and predict the energy yield of a PV system. The model can be used to develop the optimal PV system based on the location and the weather conditions. In order for bifacial PV to increase their share in the PV market, the yield prediction models have to be available in the market level. There are several models in the niche developed by research institutes such as PVSyst model, Sandia National Laboratories, EDF (Electricite De France), ISC Konstanz and Energy research Centre of the Netherlands (ECN) [5] [6] [7]. Bifacial PV yield models use elements of monofacial yield models in them, for example the temperature model and the electrical model would be fairly similar. Whereas the major difference would be the irradiance model since the bifacial models include the rear irradiance side. As the bifacial models are introduced into the market, the

investors (governments or private firms) would be more willing in making business plans around bifacial PV systems. Hence, they will play a big role in promoting the use of bifacial PV technology.

1.3 Objectives of the thesis

The objectives of the thesis are given below.

1. Study and implementation of ***ground acceptance of irradiance*** and study of ***view factors*** for the improved estimation of the irradiance incident on rear surface of bifacial panels.

2. ***Temperature analysis*** of laminates of bifacial and monofacial cells using indoor measurements.

3. Application of ***non-steady state temperature model and comparison with steady state temperature model*** used in the bifacial yield model developed at ECN for outdoor data.

4. Effect of variation in ***heat transfer coefficient*** and ***temperature*** on the annual energy yield.

The motivation for this thesis was to improve the bifacial yield model prediction by validating and introducing better methods for better prediction of the yield. The study of view factor models will be done in order to investigate if there were better models in order to predict the incident irradiance accurately. Furthermore, indoor measurements of bifacial cell laminates are conducted to understand the temperature of bifacial cell laminates in comparison with the monofacial cell laminates. Finally, the analysis of the module temperature of the bifacial panels is done for outdoor conditions and simulations to see the effect of variations in heat transfer coefficient on energy yield. These above–mentioned objectives are eventually done to provide better understanding of bifacial yield models and to give a better account of the effect of temperature on the bifacial yield output and therefore give a better idea about bifacial technology and modelling.

In chapter 2 the literature for the thesis is provided. Chapter 3 deals with the methodology and results of the rear irradiance model simulations and view factor analysis. Chapter 4 and 5 deal with temperature analysis. In chapter 4 the indoor measurements and results of bifacial cell laminate is discussed. Finally, in chapter 5 the outdoor measurements and energy yield simulations are discussed.

2 Theoretical background and Literature

In order to perform research, some basic knowledge would be required regarding the topics being worked upon. Also, it is important to understand other work in the scientific community that will be useful for better understanding and also for comparative studies for certain parts of research. Energy yield models usually consist of irradiance model, temperature model and electrical model. Other important factors such as view factors and shading (including self-shading and near field shading) which are generally part of irradiance model, have an impact on the eventual yield prediction. As explained in chapter 1.2, the bifacial yield models are not available

commercially and there are many research institutions working on developing an accurate bifacial yield model.

2.1 Rear irradiance model

The rear irradiance contributes to the output yield of a bifacial PV system and therefore it is important to estimate the irradiance on the rear accurately. The irradiance incident on the solar panel surface has three main components – direct irradiance, diffuse irradiance and ground reflected irradiance.

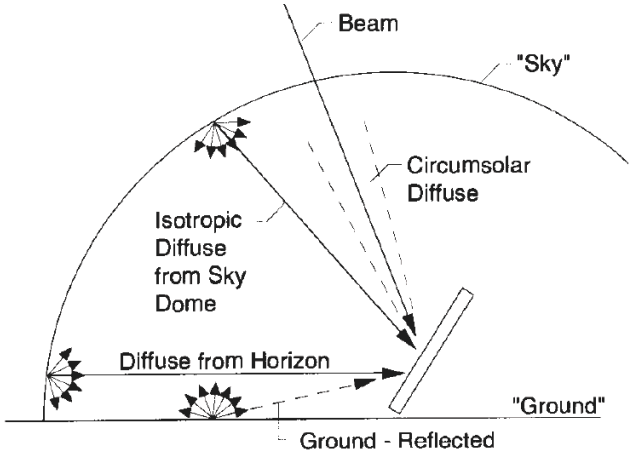

Figure 2.1 Different components of irradiance [8]

There are many irradiance models developed to estimate the incident irradiance on solar panel and they are discussed in detail in [8]. The irradiance model used in the bifacial yield model by ECN is based on the HDKR model as explained in [8]. This model is also applied in estimation of rear irradiance. The equation 2.1 describes the model, based on HDKR model, used for estimation of rear irradiance in the ECN model. Figure 2.1 shows the components involved in this model.

$$\begin{aligned} G_R = {} & (G_b + G_d A_i) R_{b,rear} f_{sh,rear} \\ & + G_d (1 - A_i)(1 + f sin^3 \frac{\beta}{2}) VF_{rear \to sky} \\ & + \rho_g (G_b + G_d A_i) \left(VF_{rear \to ground} - VF_{rear \to shed\ self\ shade} \right) \\ & + \rho_g G_d (1 - A_i) VF_{rear \to ground} \end{aligned} \quad (2.1)$$

Where $G_b R_{b,rear} f_{sh,rear}$ is the direct irradiance component.

$G_d A_i R_{b,rear} f_{sh,rear}$ is the circumsolar diffuse irradiance component.

$G_d(1 - A_i)\, VF_{rear \to sky}$ is the isotropic diffuse irradiance component.

$G_d(1 - A_i)\, VF_{rear \to sky}\, f sin^3 \frac{\beta}{2}$ is the horizon diffuse component of isotropic diffuse irradiance.

The other parts of the equation are the ground reflected components of the direct, circumsolar and isotropic diffuse irradiances.

The total irradiance, for both front and rear sides, consists of direct and circumsolar irradiance, isotropic diffuse irradiance and horizon diffuse irradiance, and lastly the ground reflected irradiance. The contribution of each of these components differs from front to rear side. For the rear side, the ground reflected irradiance contributes largely to the total rear irradiance whereas on the front side the ground reflected irradiance is less significant as compared to direct or diffuse irradiance. The figure

2.2, based on the work done at EDF by Chiodetti et al., shows the contribution of irradiance components on the front and rear side of a bifacial panel for the simulations done for the test site at EDF [9].

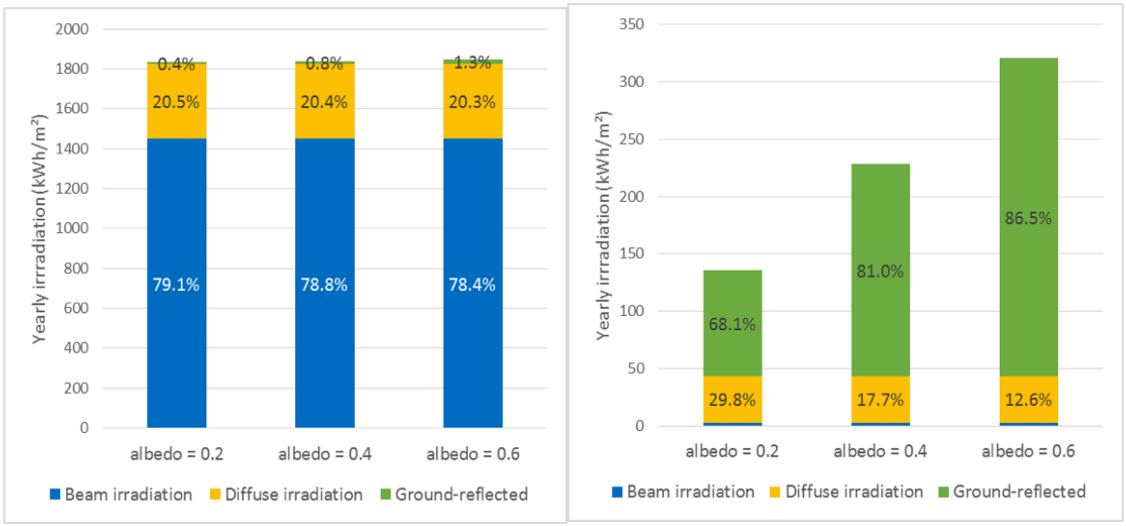

Figure 2.2 Contribution of various irradiance components for the front (Left) and rear (Right)

From the figure 2.2 it can be observed that the ground reflected irradiance has a larger contribution as compared to other components. The focus from now on will be on the estimation of the ground reflected irradiance.

2.1.1 Ground reflected irradiance

The estimation of the ground reflected rear irradiance depends on the view factor from rear surface of the panel to the ground and albedo of the ground. The bifacial panels have self-shade on the ground behind as seen in the figure 2.3. This results in absence of reflected beam and circumsolar irradiance from the shaded area. The view factor from the rear side of the panel to the ground is given in the model by Yusufoglu et al., [10]. The figure 2.3 represents the view factor from rear side of the panel to the ground. The two surfaces used in the view factor calculation are the area A_1 of the shadow and panel surface area A_2. The view factor from rear side of the panel to the ground is given by equation 2.2 based on the parameters in figure 2.3 and view factor basics.

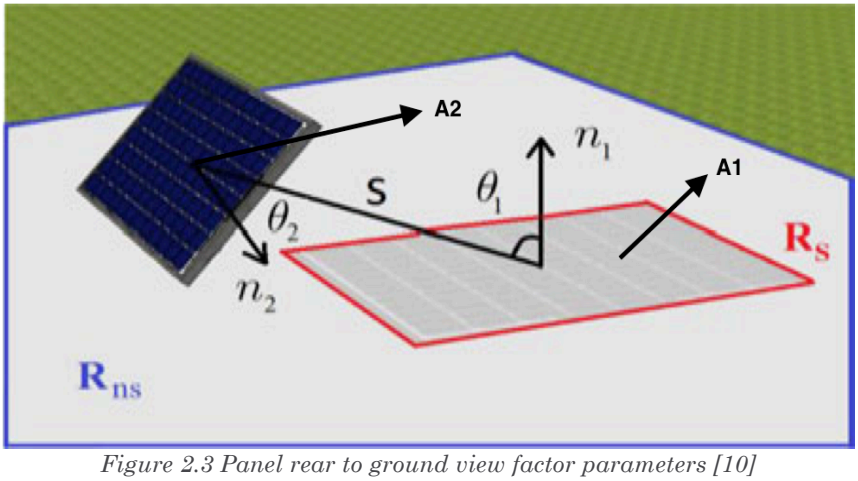

Figure 2.3 Panel rear to ground view factor parameters [10]

$$VF_{A1\to A2} = \frac{1}{A2}\int_{A2}\int_{A1}\frac{\cos\theta_1\cos\theta_2}{\pi S^2}\,dA_1\,dA_2 \qquad (2.2)$$

S is the distance between the center of the panel to center of the shaded area. The shaded area does not reflect any direct and circumsolar irradiance but only the diffuse irradiance but the irradiance reflected from the unshaded area consists of beam and circumsolar diffuse irradiance. Therefore, in order to estimate the beam and circumsolar diffuse irradiance, the view factor to the whole ground (include shaded and unshaded region) ($VF_{rear\to ground}$) is calculated and the view factor to the shaded region ($VF_{rear\to selfshade}$) is calculated. The effective view factor to estimate the reflected beam and circumsolar diffuse is the difference between the total view factor to ground and view factor to shaded area. Furthermore, each cell of the panel has different view factor due to the variation of distance, S, from each cell to the ground as a result the irradiance is spatially distributed on the rear surface. Hence, in the ECN model which used the same methodology as Yusufoglu et al., [10] the spatial results are calculated and integrated over the rear surface of panel.

This approach given by Yusufoglu et al., applies accurately to the free standing bifacial panel or shed but it does not give accurate estimate of rear irradiance for the panels in a bifacial PV system with several sheds. An alternative description for PV sheds is obtained when the irradiance reaching the ground is obstructed by the surrounding PV sheds and therefore limiting the irradiance reaching the ground surface. As seen in figure 2.2, the reflected irradiance contributes largely to the rear irradiance on the panel surface and this acceptance of irradiance determines the amount of ground reflected irradiance of different components – direct and diffuse reflected irradiance. This concept was developed by PVSyst. Also, the acceptance of the direct irradiance depends on the position of the sun and it varies with respect to the position on the ground between the panels. The elevation and tilt angle also affect the amount of direct irradiance reaching the ground. The acceptance for the diffuse reflected irradiance is determined by the amount of sky as seen by the ground and it depends on the tilt angle of the panels and elevation [11]. Figure 2.4 below shows the beam irradiance accepted by the ground and its variation with sun position and figure 2.5 shows the diffuse (isotropic) irradiance acceptance by the ground and its variation with the elevation [11].

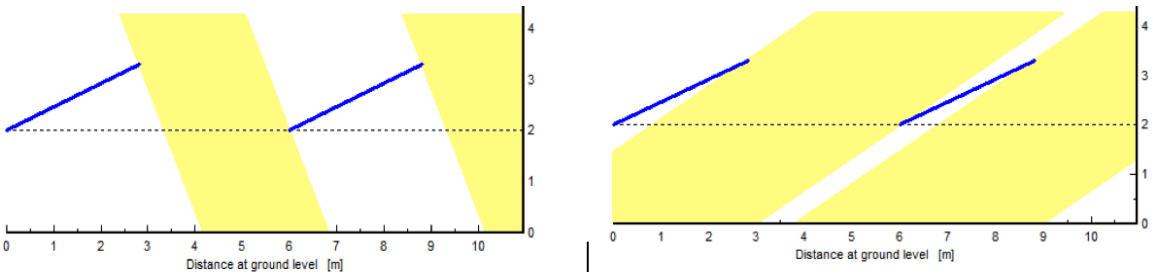

Figure 2.4 Left: Geneva 21st June 12:00 h and right: Geneva 21st June 19:00 h [11]

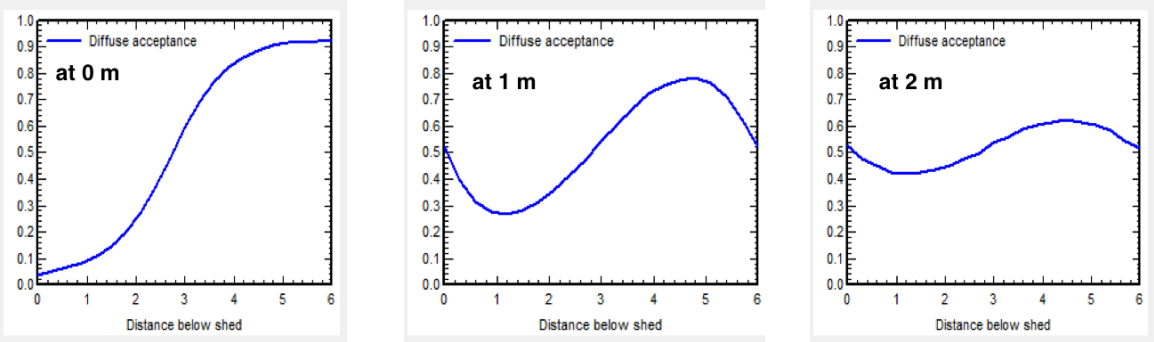

Figure 2.5 Diffuse irradiance acceptance variation with distance at three different elevations [11]

This method is essentially a 2D model and the ground behind the shed is divided into several strips. Each strip of the ground is calculated to have different acceptance as seen in figure 2.5 (variation of acceptance with distance below shed). In this method after the calculation of the ground acceptance of each strip, the view factor of the panel to the section of the ground is calculated. Therefore, the rear irradiance depends on the product of view factor, ground acceptance and albedo as given in the equation 2.3 for reflected isotropic diffuse irradiance and equation 2.4 for reflected beam and circumsolar diffuse irradiance.

$$G_{R,refID} = \rho_g G_d (1 - A_i) \sum_{i}^{n\ strips} VF_{rear \rightarrow ground}(i) \bullet Acc_{iso}(i) \tag{2.3}$$

$$G_{R,ref\ beam+CS} = \rho_g (G_b + G_d A_i) \sum_{i}^{n\ strips} VF_{rear \rightarrow ground}(i) \bullet Acc_{beam+CS}(i) \tag{2.4}$$

The reflected beam and circumsolar diffuse components for a stand-alone bifacial panel is given by equation 2.5 based on the Yusufoglu et al., methodology. As there is no obstruction due to surrounding sheds or panels, the acceptance of beam and circumsolar diffuse is only determined by the self-shaded area.

$$G_{R,ref\ beam+CS} = \rho_g (G_b + G_d A_i) \sum_{i}^{n\ strips} VF_{rear \rightarrow ground}(i) - VF_{rear \rightarrow selfshade} \tag{2.5}$$

2.1.2 View factors – Diffuse and ground reflectance

The view factor is an important parameter in determination of the irradiance. The amount of diffuse irradiance and ground reflected irradiance incident on the solar panel surface depends on their respective view factors – solar panel to sky VF and panel to ground VF in the equations 2.6 and 2.7 [8]. It should be kept in mind that while calculation of view factors for the rear side the tilt angle would be $(\pi - \beta)$.

$$VF_{f \rightarrow sky} = \frac{1 + cos\ (\beta)}{2} \tag{2.6}$$

$$VF_{f \rightarrow ground} = \frac{1 - cos\ (\beta)}{2} \tag{2.7}$$

The contribution of the ground reflected irradiance to the total irradiance on the front side is very low, therefore it is not being studied. Most of the literature is based on the reference of the work of J. Appelbaum [12] and the equations used in the ECN model for bifacial yield prediction.

2.1.3 Front to sky view factor: Diffuse isotropic irradiance

As explained above, the general equation of view factor of the front of a panel facing the sky is given by equation 2.6. This applies for panel that does not have any obstruction by another panel in front of it. The figure 2.6 depicts the scenario where the panel in the front obstructs the view factor to sky which leads to its reduction as it area of sky seen by the panel reduces.

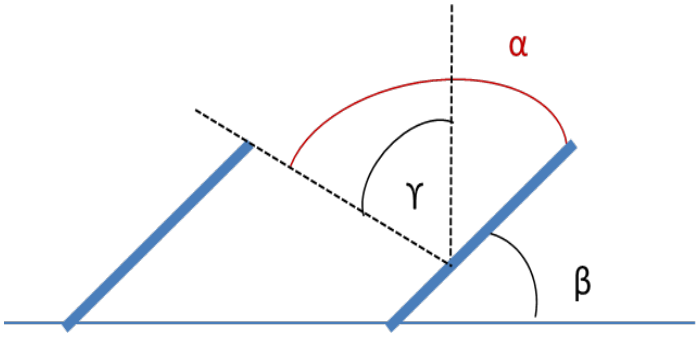

Figure 2.6 Parameters in calculation of view factor from panel to sky

In the model at ECN, the front to sky view factor was calculated based on the equation 2.8 given below. The ECN model uses this method in which the sky dome is split into two halves at the zenith and the view factor is calculated for the two angles γ and $\frac{\pi}{2} - \beta$.

$$VF_{f\rightarrow sky} = \frac{\sin(\gamma) + cos\ (\beta)}{2} \tag{2.8}$$

The angle γ depends on the position from which the view factor is calculated and therefore the view factor is different for various positions along the panel.

From the work of J. Appelbaum in [12], the view factor is calculated in a different way where as opposed to the ECN model method, it uses one angle, α. The view factor is by this method is given in equation 2.9. From the figure 2.6 it is also clear that the angle α depends on the tilt angle β.

$$VF_{f\rightarrow sky} = \frac{1 + cos\ (\pi - \alpha)}{2} \tag{2.9}$$

Since the trigonometric functions are not linear, the sum of trigonometric functions of two half angles in not equal to the trigonometric function of the full angle. The method given by Appelbaum is more logical as it uses the whole view factor angle instead of two separate angles.

2.1.4 Rear to sky view factor: Diffuse isotropic irradiance

For the rear to sky view factor which determines the amount of diffuse irradiance reach the rear side from the sky is also generally obstructed by the panel behind. The

figure 2.7 describes the scenario for which ECN model calculates the view factor as given by the equation 2.10.

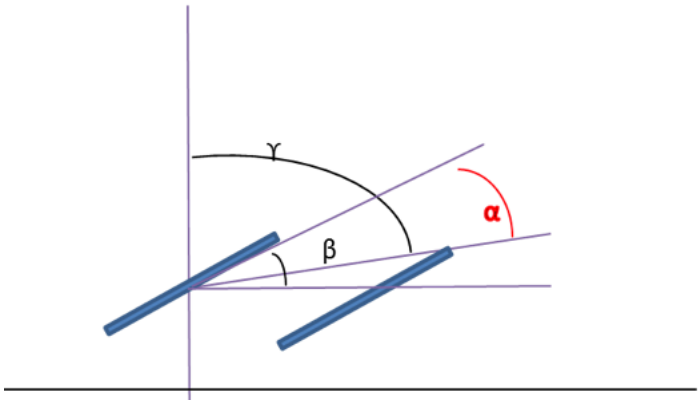

Figure 2.7 View factor figure for rear to sky

$$EF_{r\to sky} = \frac{\sin(\gamma) - cos\ (\beta)}{2} \tag{2.10}$$

Now again, the view factor described by Appelbaum uses the full angle α for the rear and therefore, equation 2.9 is used here as well but the angle α would be different for the rear side.

2.1.5 Rear to ground view factor: Reflected irradiance

The calculation of the view factor for the rear to ground reflected irradiance in the ECN model is based on the method by Yusufoglu et al [10]. This is explained in the section 2.1.1 – ground reflected irradiance.

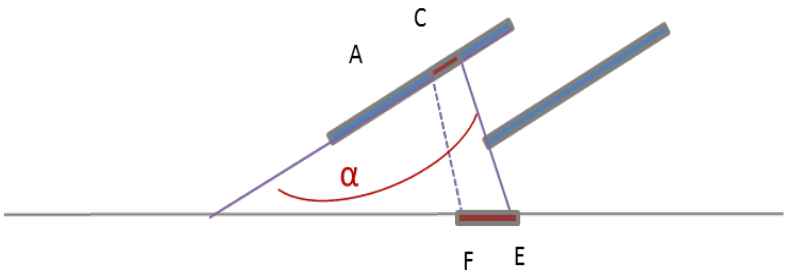

Figure 2.8 Panel to ground view factor for rear side

Again, using the method suggested by Appelbaum, the view factor is calculated differently as compared with the method used in ECN model. The angle α again would be different for this scenario as seen in figure 2.8 and using view factor equation of 2.9 the rear side view factor from panel to ground can be calculated.

In all the above-mentioned methods, the elevation does not play a role in calculation of view factor but in reality, it does. Appelbaum gives the rear to ground view factor based on the figure 2.9 and using the cross-string rule, equation 2.11 is derived [12]. Now rewriting the equation in terms of the dimension of the panel's setup equation 2.11 is derived.

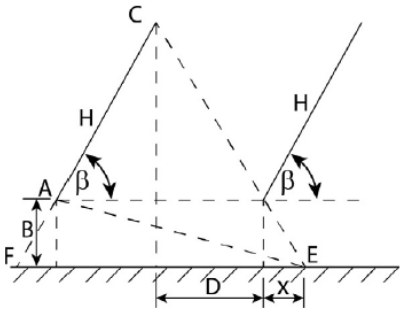

Figure 2.9 2D model depicting the various parameters in calculation of $AF_{r\rightarrow gr}$

$$VF_{r\rightarrow gr} = \frac{H + [B^2 + (Hcos\beta + D + X)^2]^{\frac{1}{2}} - [(D + X)^2 + (Hsin\beta + B)^2)]^{\frac{1}{2}}}{2H} \tag{2.11}$$

The effect of elevation had not been implemented initially and the certain analysis done on the rear to ground view factor will be discussed in the section 3.1.

2.2 Module temperature

The operating temperature of the solar modules/panels has an effect on their performance. The ambient temperature itself increases as the irradiance increases through a day. Therefore, it is expected that as the irradiance and ambient temperature increases, the module temperature also increases [13].

2.2.1 Effect of temperature on electrical parameters

The module temperature only has a small effect on the short-circuit current. With increase in temperature, the short-circuit current increases slightly. The open-circuit voltage, V_{OC}, is highly affected by the increase in temperature. The temperature dependency is given by the equation 2.12 below [14].

$$\frac{dV_{OC}}{dT} = -\frac{V_{go} - V_{oc} + \gamma_i \left(\frac{kT}{q}\right)}{T} \tag{2.12}$$

The fill factor is reduced due to decrease in the V_{OC} with temperature increase and therefore resulting in the decrease in the total power output [14].

2.2.2 Heat transfer coefficient

The heat transfer process is the transfer of heat from a hot body to a cold body. It is known that the heat transfer process occurs through three different processes namely conduction, convection and radiation. In the conduction process the heat is transferred when the hot body and cold body are in contact and the heat is transferred through the molecules of hot body to the cold body. In convection, the heat is transferred through a fluid in motion from a hot body to its surroundings. Radiation, unlike conduction and convection, is a process in which the heat is transferred in the form of electromagnetic radiation. The heat transfer coefficient gives the amount heat

transferred per unit area from one point to another point for a temperature difference of 1 K. Generally, the contribution of conduction in heat transfer is ignored [15].

The energy balance equation for a solar panel can be described by the equation 2.13 below [13]. In this equation, the heat exchange (heat flux) due to convection and radiation is considered. The last two terms on the right-hand side of the equation are due to the contribution of radiation at both front and rear surfaces of a solar panel.

$$t\rho C_p \frac{dT_m}{dt} = Q_{in} - h_c(T_m - T_a) - \epsilon_f \sigma\left(T_m^4 - T_{sky}^4\right) - \epsilon_r \sigma\left(T_m^4 - T_{ground}^4\right) \qquad (2.13)$$

In the equation 2.13 per unit area values of heat input is used. There are many models present in the scientific literature to calculate the heat transfer coefficient and one such dynamic model is based on the equation 2.13. Furthermore, the method described in Hoang et al [16] calculates the energy balances for each layer in a PV module in order estimate its temperature. In the steady state model used in ECN model, the heat transfer coefficient contains the effect of convection and radiation in one single value, U. The energy balance equation after this assumption is made, is explained in next section.

2.2.3 Module temperature estimation models

There are several temperature models available to estimate the operating temperature of the modules. Of the available models, **NOCT (normal operating cell temperature) model** is a basic and simple steady state approach to determine the module temperature. The NOCT values of a PV panel are provided in the datasheet by the manufacturing companies. The NOCT value of a PV panel is determined under specific conditions of irradiance of 800 W/m^2, at an ambient temperature of 20 ºC, assuming a constant overall heat transfer coefficient and at wind speed of 1 m/s. The module temperature based on this model is given in equation 2.14 [17].

$$T_m = T_a + (NOCT - 20℃)\frac{G_M}{800\ W/m^2} \qquad (2.14)$$

But the **energy balance equation** is far more dynamic than the steady state models to estimate the module temperature. The dynamic energy balance equation is given below in 2.15.

$$t\rho C_p \frac{dT_m}{dt} = Q_{in} - U(T_m - T_a) \qquad (2.15)$$

Solving the differential equation above results in the following equation and applying boundary conditions,

$$T_m(t) \quad = T_a + \frac{Q_{in}}{U} - \left(\frac{Q_{in}}{U} - T_a + T_o\right) \bullet e^{-\frac{U}{t\rho C_p}t} \qquad (2.16)$$

Boundary condition being $T_c(0) = T_o$, where T_o is the initial temperature of the module and sometimes it can be same as the ambient temperature. This above equation is true for a constant input of irradiance and ambient temperature but during the day these two are very much variable. Therefore, for time duration of Δt, the above equation is true. Assuming that for every time interval of Δt, the input

variables (irradiance and ambient temperature) change and therefore module/cell temperature also changes.

$$T_{m\,(i-1)} \xrightarrow[\Delta t]{} T_{m\,(i)} \xrightarrow[\Delta t]{} T_{m\,(i+1)}$$

We know that at boundary condition t=0, the cell temperature ($T_{c\,(i)}$) is equal to the previous cell temperature ($T_{c\,(i-1)}$), hence, applying the boundary condition to the equation above results in the following equation,

$$T_{m\,(i)}(\Delta t) = T_a + \frac{Q_{in}}{U} + (T_{m\,(i-1)} - T_a - \frac{Q_{in}}{U}) \bullet e^{-\frac{U}{t\rho C_p}\Delta t} \tag{2.17}$$

With the availability of the module heat capacity, and heat transfer coefficient, this energy balance equation is used in prediction of the module temperature.
The **ECN bifacial yield** model utilizes the steady state energy balance model. This model is the same model used in the PVSyst software [18]. The model equation is given in 2.17.

$$T_m = T_a + \frac{Q_{in}}{U} \tag{2.18}$$

where, U is calculated as given in equation as 2.17.

$$U = U_c + U_v \bullet v \tag{2.19}$$

where, U_c is a constant convective heat transfer coefficient.
U_v is a heat transfer coefficient value as a function of wind speed (v).
The values of U_c and U_v for the ECN model were taken from the PVSyst database which is based on the Faiman model [19]. Both values were determined based on the measurements. The U_c and U_v values are given in the table 2.1 which are different for different configurations as recommended by PVSyst [18].

Table 2.1 U_c and U_v values recommended by PVSyst

Case	U_c [W/m²•K]	U_v[W/m²•K/m/s]
Free standing	29	0
Intermediate	20	0
Fully insulated back	15	0
Based on user data	25	1.2

It has also proposed values based on some user measurements measured in the mainland (low wind speed) and not at coastal areas (high wind speed). The ECN model uses higher U_v value since the simulations are based in the Netherlands (high wind speed region).

3 Rear irradiance and view factor analysis

The view factors were part of the irradiance model in the ECN model for the bifacial energy yield prediction. In this chapter, the view factors used by the ECN model are evaluated and compared to the other view factor models developed by J. Appelbaum.

3.1 Simulations for ground acceptance of the irradiance

In order to see the results of the rear irradiance under the condition of tilt angle being 0º and elevation being 0 m (panel placed flat on the ground surface), the simulations were done. The details of the location and system are given in table 3.1. The system contained 7 sheds, each shed consisting of 25 columns and each column consisting of 4 panels. The simulations were done for a single day – July 1st.

Table 3.1 System configuration for simulations

System Parameter	Details
Location	Vaassen, the Netherlands
Initial Tilt	0º
Initial Elevation of panels above the ground	0 m
Albedo	20 %
System size	700 Panels (4×25×7)

The rear irradiance is expected to be zero but the results of the simulation for that condition showed presence of irradiance on the rear side and to be very high as seen in the table 3.2 below. The simulation output resulted in high reflected diffuse circumsolar and isotropic components. As the panel is facing the ground, only reflected irradiances reach the rear. In practice, at the elevation of 0 m and 0º tilt angle, the ground effectively acts as a backsheet and the irradiance reaching the rear side of the panel is very low (close to zero).

It was explained in the literature on the ground reflected irradiance in 2.1.1, the ECN model uses the Yusufoglu method to calculate the view factor from rear to ground. At the elevation of 0 m and 0º tilt angle, the reflected irradiance is estimated to be high which is due undefined calculation of view factor from rear to ground which is due to the condition $S \rightarrow 0$ in the equation 2.2.

The reflected irradiance depends on the amount of irradiance 'accepted' by the ground to be reflected and the rear irradiance model was modified based on the ground acceptance literature as explained in section 2.1. The changes were made such that the acceptance of irradiance depends on tilt angle, elevation of the bifacial panels, the position of the sun and position on the ground.

Table 3.2 Rear irradiance on the rear side of the panels

	G_R [Wm^{-2}]	$G_{R,ref\ DCS}$ [Wm^{-2}]	$G_{R,ref\ ID}$ [Wm^{-2}]
Before correction	1174.4	768.04	406.37
After correction	4.30E-13	4.30E-13	0

As seen in the figure 3.1 and 3.2, which give the total rear irradiance in a day on a bifacial PV panel at variable tilt angle and elevation respectively. The figures show the rear irradiance variation before and after correcting and implementing the view factor corrections.

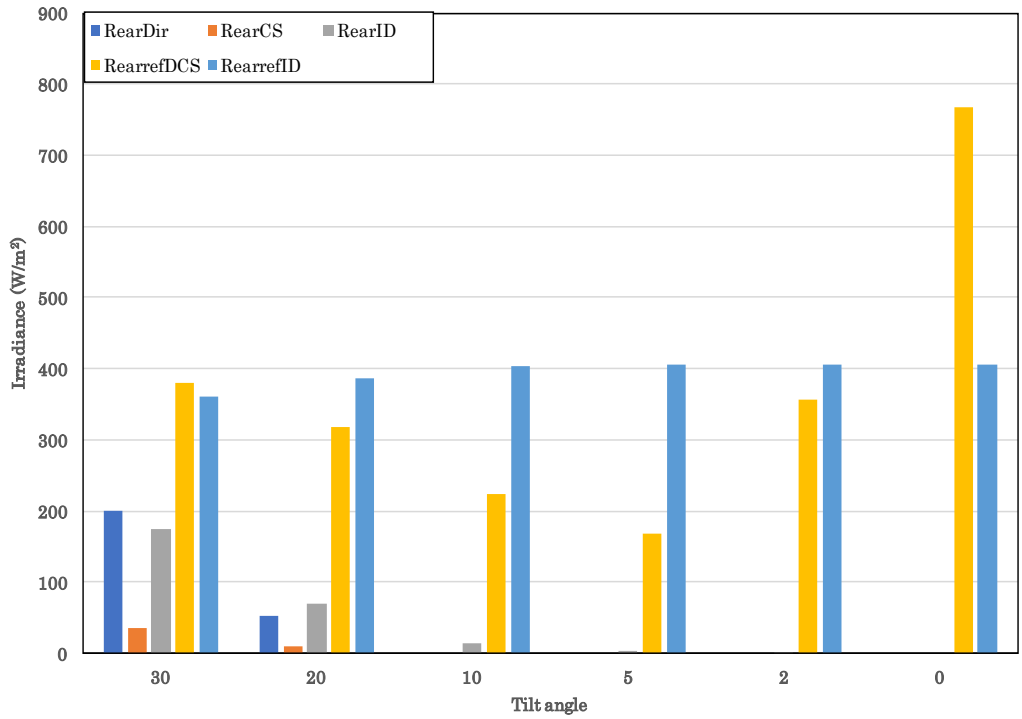

Figure 3.1 Variation in rear irradiance with tilt angle before model correction and at 0 m elevation

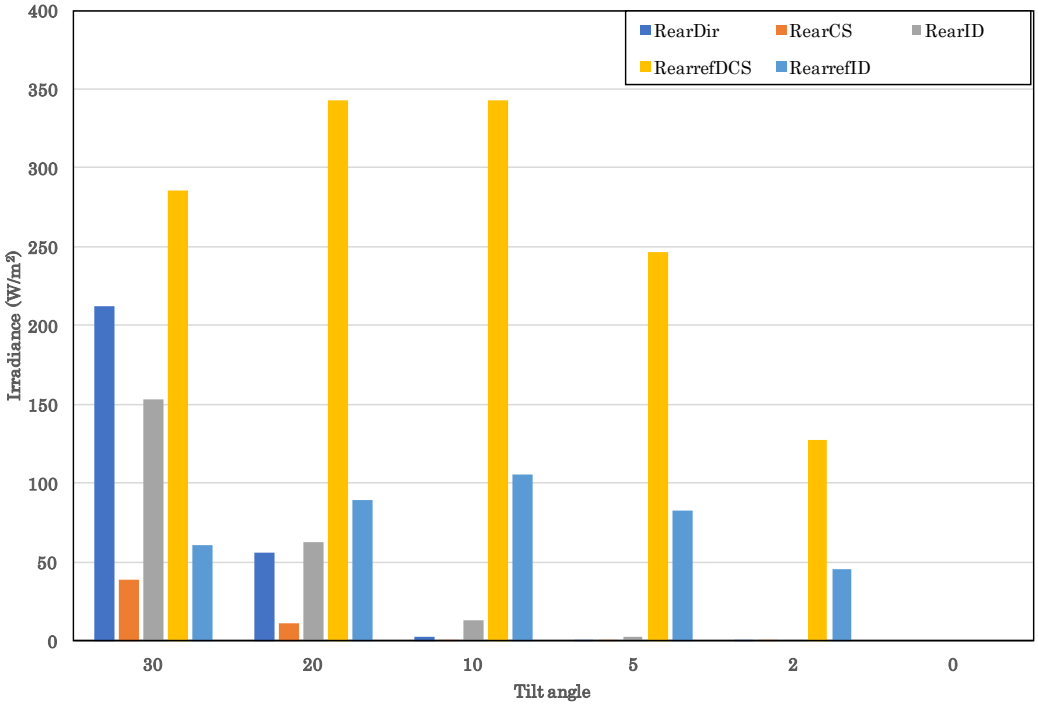

Figure 3.2 Variation in rear irradiance with tilt angle after model correction and at 0 m elevation

As seen in the figures 3.1 and 3.2 the results after the modifications in the model were made and the variation of rear irradiance for the varying tilt angle are given. Comparing the two figures, it can be seen that the reflected irradiance is decreased considerably, including the reflected beam and circumsolar diffuse irradiance and reflected isotropic diffuse irradiance. Therefore, it can be seen that the model behaves as expected by incorporating the ground acceptance concept. This is also reflected in the figures 3.3 and 3.4 for the variation in elevation. From both the figures the rear irradiance is very low when the panels are flat and close to the ground.

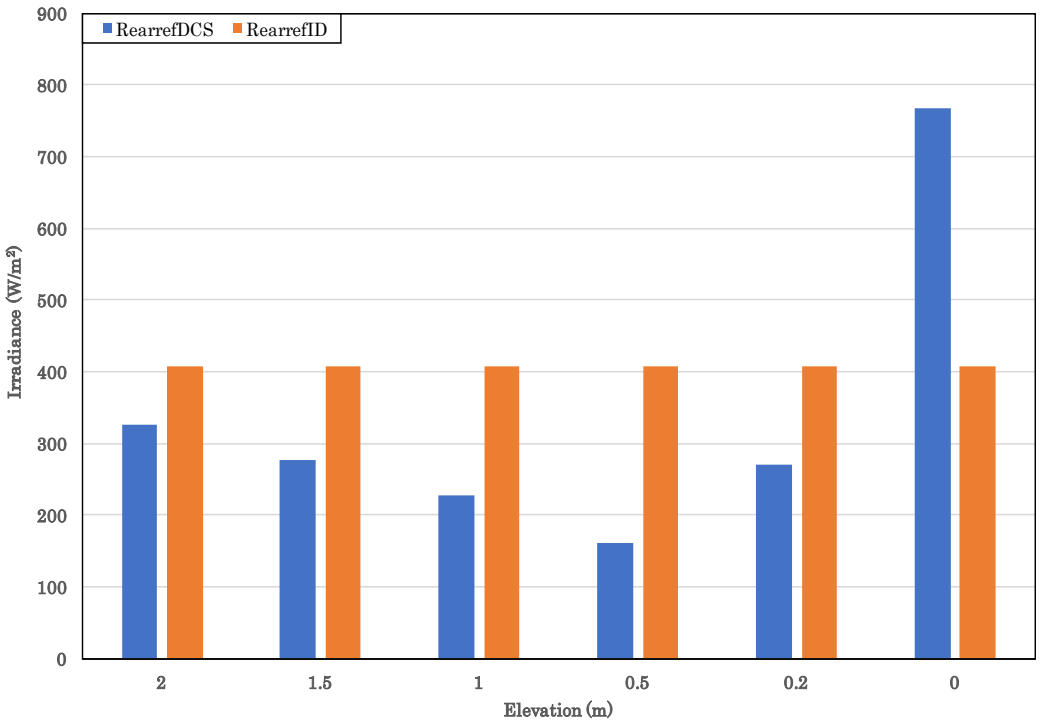

Figure 3.3 Variation of rear irradiance with elevation before model correction at 0 tilt angle

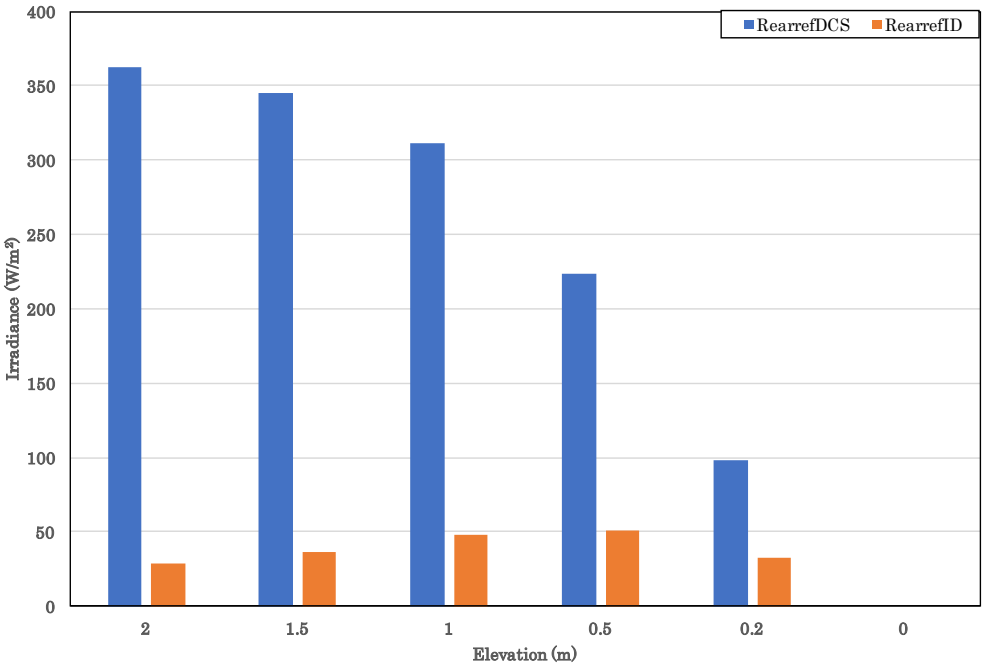

Figure 3.4 Variation of rear irradiance with elevation and after model correction at 0 tilt angle

3.2 Validation of rear irradiance model with outdoor data

The test site on the rooftop of the solar building at ECN has the setup for a bifacial panel of glass-glass type and also one with a white backsheet. The three panels used in the outdoor measurements are given in the table 3.3. The setup established at the ECN did not include the Al-BSF monofacial panels therefore only the different panels with bifacial cells were considered. The setup details of the three panels on the rooftop is given in the table 3.4.

Table 3.3 Panels used for outdoor analysis

Shorthand	Cell Technology	Cell type	Backsheet
B510	Bifacial	n-PERT	Glass
B511	Bifacial	n-PERT	Glass + White in non-active area
B512	Bifacial	n-PERT	White + Aluminum

Table 3.4 Orientation details of the panels

Tilt	30º
Azimuth	0º (South facing)
Elevation	0.3 m
Albedo	30 %

The panels are connected to the measurement devices of irradiance, current, voltage, and module temperature. Also, two rear irradiance measurement devices are placed such each one is present between two panels. Therefore, the rear irradiance may not be exactly accurate. Also, the effect of self-shading and near-field shading have to be taken into account. These effects also lead to only a fair approximation of the actual rear irradiance incident on the panel. The measurement of the electrical parameters was done using the IV tracer developed at the ECN and the temperature was measured using the PT100 sensor. The system was assumed to be free standing. The irradiance on the rear side was simulated for meteorological data of June 11th. The results of the simulation and measurements are given in figure 3.5 for validation of irradiance model with measured data. The albedo of 30 % was assumed due to the ground being a mixture of concrete (grey) and white paint.

The model modifications not only include the ground acceptance term but also the view factor calculation method. In the literature, the method described by J. Appelbaum is described and this method is implemented in the view factors' calculation. This is due to the simplicity of the Appelbaum's method as it assumes the view factor to be same for a horizontal strip of cells in the panel [12]. Therefore, the new model calculates the view factor of each horizontal strip in a panel and the ground acceptance of each strip of ground. Combining the effects of these two modifications the results are much more realistic and simpler to estimate the rear irradiance.

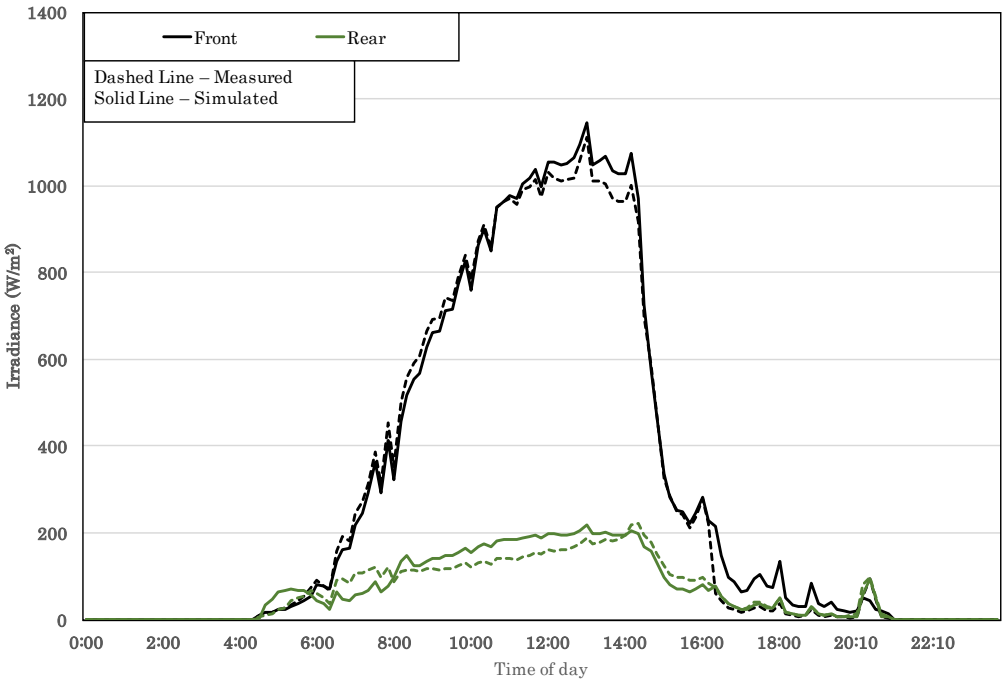

Figure 3.5 Model results of June 11th compared with the measured values

4 Indoor measurements

Indoor measurements were done in order understand the temperature characteristics of single cell monofacial and bifacial modules (or laminates). The measurements were done at a lab in ECN using the Large area solar simulator (LASS) by Eternal Sun [20].

4.1 Setup and methodology

The indoor measurements of six single cell solar modules were done of which three were bifacial cell type and three were monofacial cell type. The monofacial cell laminates were used in this experiment for comparison with the bifacial cell laminates. Each of the six modules were tested separately under the Eternal sun. The table 4.1 gives the different modules used for the measurements. The active area of the bifacial cell and monofacial cell laminates is 239 cm^2 and 243.4 cm^2 respectively. All the six modules have total area of 400 cm^2.

Table 4.1 Solar modules used for the indoor experiments and measurements

Cell Type	Cell Technology	Module Type	Backsheet	Shorthand
Bifacial	PERPoly	Bifacial	Glass	BG
Bifacial	PERPoly	Monofacial	White	BW
Bifacial	PERPoly	Monofacial	Black	BB
Monofacial	Al-BSF	Monofacial	Glass	MG
Monofacial	Al-BSF	Monofacial	White	MW
Monofacial	Al-BSF	Monofacial	Black	MB

These six modules were selected in order to figure out the differences not only between the bifacial and monofacial cell technology but also the differences in terms

of rear cover (glass or backsheet) used. It can be expected that the bifacial cell with white backsheet results in higher electrical performance than the bifacial cells with glass or black backsheet due to the extra irradiance reflected and scattered from the white backsheet [21]. Whereas the bifacial cell with the black backsheet is more aesthetic but the performance might not be as good as the other two (BW and BG) due to high heat absorption. Additionally, the monofacial modules were also selected to comparatively analyze the difference between the two technologies. Therefore, these modules were selected for the measurements.

The measurements of electrical parameters – current and voltage – of the solar module were done using the I-V tracer device and software developed at the ECN. This device is also used for the measurement of both ambient and module temperature. The module temperature is measured using the PT100 temperature sensor and it is attached at the rear side of the active area of the solar module. The IV tracer device measures short-circuit current, open circuit voltage, current and voltage at maximum power point. The measurements are then recorded on the software and can be saved for analysis.

The ambient temperature of the room was 23 ºC and the irradiance of solar simulator was set at 1000 W/m^2. The ground of the experiment room was covered by a carpet of a dark grey color which has a very low reflectance and hence the rear irradiance on the modules is negligible. All the modules were measured under these conditions. A manually set time interval between two sets of measurements is required to be set in the measurement software. During each experiment an interval of 10 seconds was chosen between two measurement sweeps. This was done in order to get an accurate behavior of changing module temperature with time. The duration of each experiment was 40 minutes. It was chosen such that it covers the variation of the module temperature from initial ambient temperature to its steady state temperature.

4.2 Results and Discussion

4.2.1 Temperature measurement analysis

The irradiance from the solar simulator was measured using a reference solar cell of c-Si type. The irradiance produced by the solar simulator was found to be close to 1200 W/m^2. It was not possible to determine the actual reason as to why the extra 200 W/m^2 was produced by the simulator. Due to this, an increase in the steady state temperature due to its linear relationship with the irradiance given by equation 2.18.

The heat input depends the amount of the incoming irradiance absorbed by the solar module. Part of the incoming irradiance also is reflected and transmitted by the module and the rest of it is absorbed by the solar module. Some part of the absorbed irradiance is converted into electrical energy and the remaining leads to heating up of the module. The heat input, Q_{in}, for bifacial solar modules is calculated using the equation 4.1.

$$Q_{in} = \alpha_f \bullet G_f \tag{4.1}$$

The absorption for front side, α_f, is calculated using the equation 4.2 below.

$$\alpha_f = 1 - R - T - \eta \tag{4.2}$$

The rear contribution is present for the bifacial modules in the outdoor environment and the contribution of rear irradiance is absent for the case of indoor measurements but it also depends on the albedo of the ground in the indoor conditions.

Reflectance (R) and transmission (T) values were calculated for each module using the measured data available at ECN as a result of work of my colleague Ebrar Ozkalay. Also, the efficiency of each module was calculated at standard test conditions. Therefore, using these values, the heat input for each module was estimated. The table 4.2 below shows the reflectance, transmission, STC efficiency and heat input (Q_{in}) for the active area.

It has to be noted that during the measurements, the modules did not have same initial temperatures. This was due to time taken due to setting up each module under the simulator and also the small amount of time to change the name of the measurement records in the software. The module that was worst affected by this was the bifacial module with black backsheet. Therefore, in order for good comparison of temperature behavior among the modules, the temperatures of only above 32 ºC were considered. Another important discrepancy to be noted is the behavior of monofacial glass module. This dip in temperature from the 500–seconds point is due to the fact that at the moment the solar simulator light source had been turned off and therefore, the measurement had to be stopped for a little while and hence the dip in the temperature.

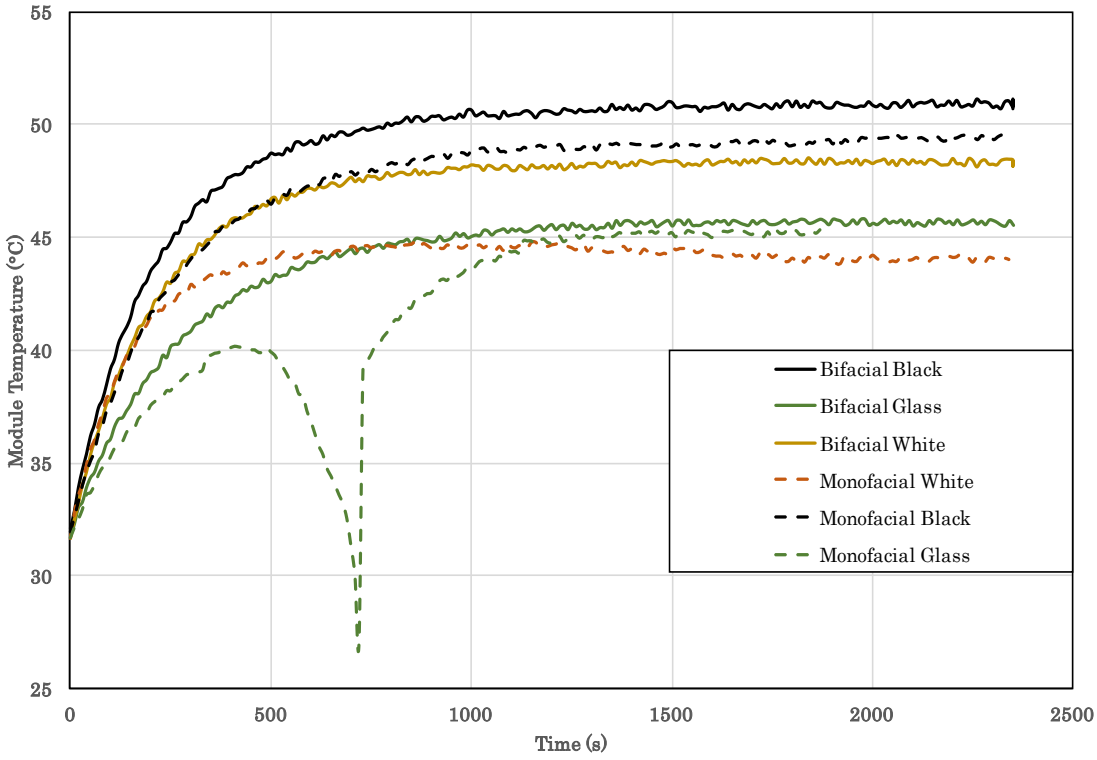

Figure 4.1 Variation of module temperature of six modules

The varying module temperatures of the six solar modules are shown in the figure 4.1. Firstly, as expected both cell laminates having black backsheets (BB and MB) have higher temperatures as compared to the other four cell laminates. This is due to the high absorption of the irradiance by the color black. The temperatures of the three bifacial cell laminates correlate to the amount of irradiance absorbed by active area. As expected, the BW laminate has higher temperature as compared to the BG laminate due to the fact that it has absorbs the extra irradiance reflected off the white backsheet.

Table 4.2 Reflectance, transmission, efficiency and heat input values of solar modules

Cell Laminate	Reflectance	Transmission	α	η at STC [%]	Q_{in} [W/m²]
BG	0.113	0.11	0.663	10.7	798
BW	0.137	0.04	0.703	11.7	846
BB	0.11	0.03	0.757	10.3	889
MW	0.121	0	0.771	10.83	931
MB	0.125	0	0.775	9.97	930
MG	0.12	0.05	0.73	10.1	876

The three bifacial solar cell modules reach a higher steady state temperature as compared to their monofacial counterparts as seen in figure 4.1. This result is quite unexpected since the monofacial cell laminates absorb higher irradiance as seen in the table 4.2. However, the temperature sensor measures the temperature at the rear cover of the laminate and not of the cell. In the case of bifacial cell laminates, the irradiance transmitted through the cell hits the backsheet directly and for the monofacial the irradiance absorbed is conducted to the rear cover through the EVA. The temperature of the MW laminate decreases slightly around 20 minutes which could be due to failure of sensor or the ambient conditions. For the initial part of figure indicate the temperature of the monofacial cell laminates have similar order as the bifacial cell laminates i.e. MB>MW>MG. The differences in the monofacial cell laminates could be attributed to the difference in the non-active areas of the cell laminates. In conclusion, even though the monofacial cell laminates absorb higher irradiance, this is not reflected in the temperature measurements at the rear of the laminates.

4.2.2 Effect of temperature on the electrical parameters

As explained in the section 2.2, the effect of temperature is prominent on the V_{OC} and not so much on I_{SC}. In the figure 4.2 the I_{SC} of the six cell laminates are not affected with increasing temperature. The current increases with increase in the irradiance [13]. As observed in the figure, the BW laminate has the highest current due to the white backsheet at the rear and is also explained in [21]. The stray rear irradiance on the back of the BG laminate adds to the total I_{SC} and therefore it has higher current as compared to the BB laminate this is also in agreement with the STC values in the table 4.3. Also, for the MW laminate, the extra reflective white surface leads to extra contribution of irradiance to the I_{SC} as it is also seen in the STC values. The I_{SC} of MB laminate is higher as compared to the I_{SC} of MG due to the effect of higher temperature on the MB laminate.

Table 4.3 V_{OC} and I_{SC} STC values of six laminates

Cell Laminate	V_{OC} [V]	I_{SC} [A]	$\frac{dV_{OC}}{dT}$ [V/K]
BG	0.676	8.92	0.00201
BW	0.679	9.49	0.002
BB	0.674	8.73	0.00201
MG	0.629	8.59	0.00216
MW	0.626	8.93	0.00217
MB	0.63	8.53	0.00216

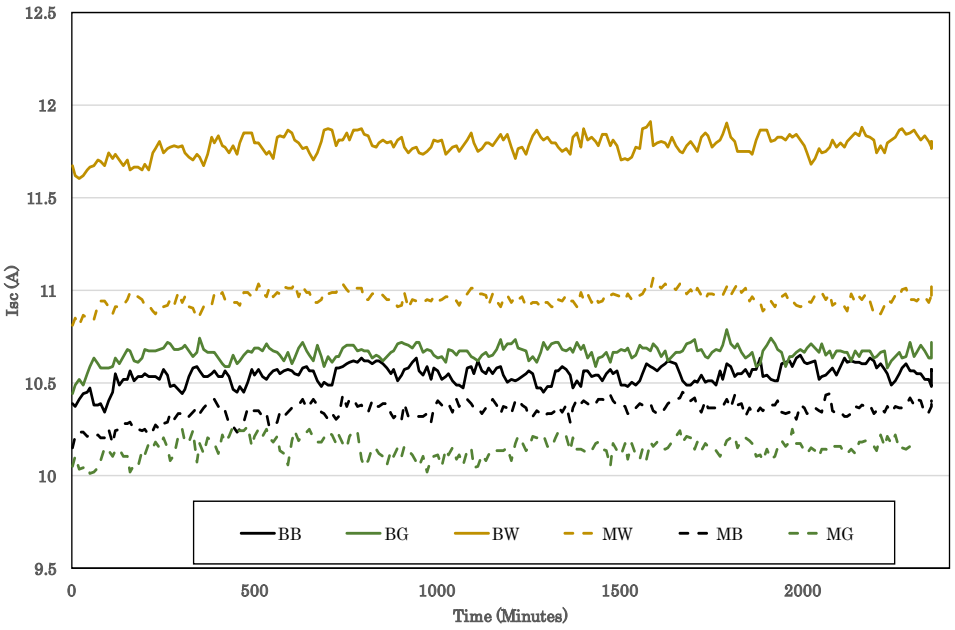

Figure 4.2 I_{SC} of the six modules

In the figure 4.3 the open circuit voltage of the six cell laminates can be observed. The V_{OC} values are decreasing with time, indicating the increase in temperature. In figure 4.1 the differences in rear side temperature among BB, BW and BG laminates are noticeable whereas from the figure 4.3 the differences in V_{OC} are very minimal. The V_{OC} variation among the monofacial cell laminates is however, is clearer.

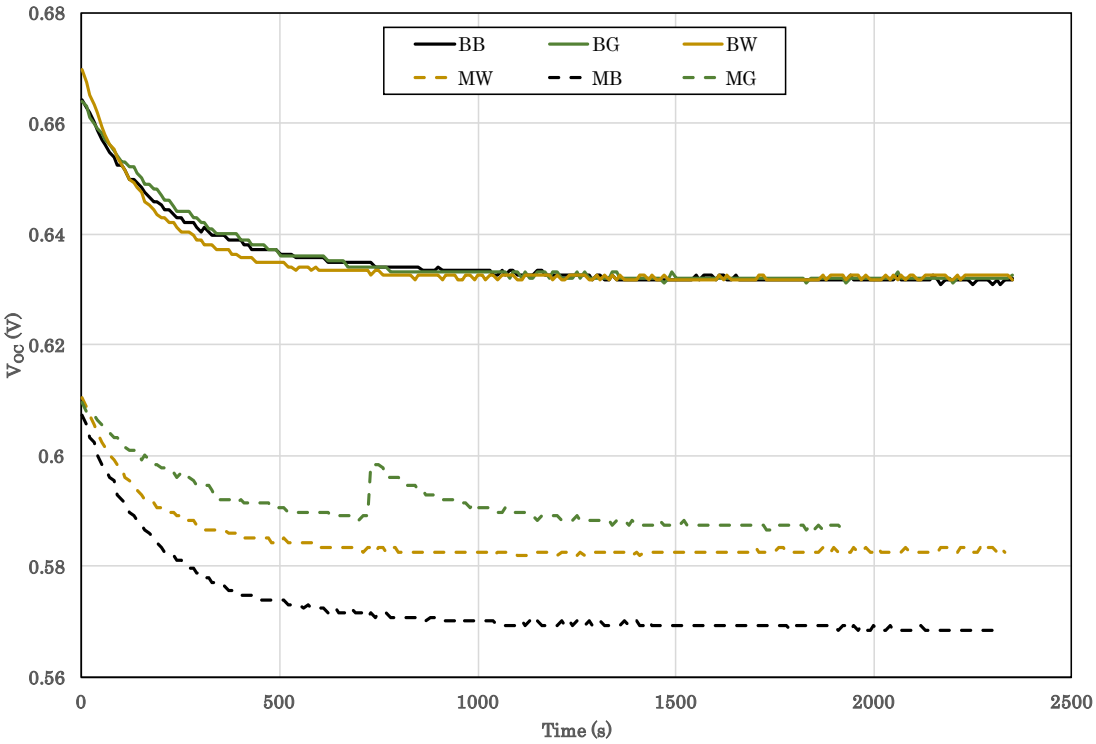

Figure 4.3 V_{OC} of the six modules

4.2.3 Comparison of measured temperatures with Voc temperatures

In order to see the difference between the measured and Voc temperatures, the temperatures of the cells based on their Voc were calculated using the equation 4.4 and 4.5, using the Isc and Voc measurements shown in figures 4.2 and 4.3 respectively. The Voc is adjusted for the irradiance (using current due to its linear relationship with irradiance) and then the temperature is calculated using the measured $V_{OC}(T_m, G_{STC})$.

$$V_{OC}(T_{STC}, G_m) = V_{OC,STC} + \frac{nkT}{q} \ln\left(\frac{I_{SC,m}}{I_{SC,STC}}\right) \tag{4.4}$$

$$V_{OC}(T_m, G_{STC}) = V_{OC,STC} + \frac{dV_{OC}}{dT}(T_m - T_{STC}) \tag{4.5}$$

The $\frac{dV_{OC}}{dT}$ values were calculated using the equation 2.14 for each cell laminate and are given in table 4.3. The measured and Voc temperatures of laminates with bifacial cells and monofacial cells are given in figures 4.4 and 4.5 respectively. Generally, the cell temperatures are expected to be higher than the measured temperatures (module temperatures). As expected, this applies for both BW and BG laminates but it is not the case for the BB as seen in the figure 4.4. This reason for the higher measured temperatures could be due to the high absorption of irradiance by the black backsheet, in particular the inactive area. Therefore, the temperature of the backsheet could have been higher than the cell itself. The cell temperatures of the BG and BB laminates have a small difference between then given the small differences between their Voc and Isc.

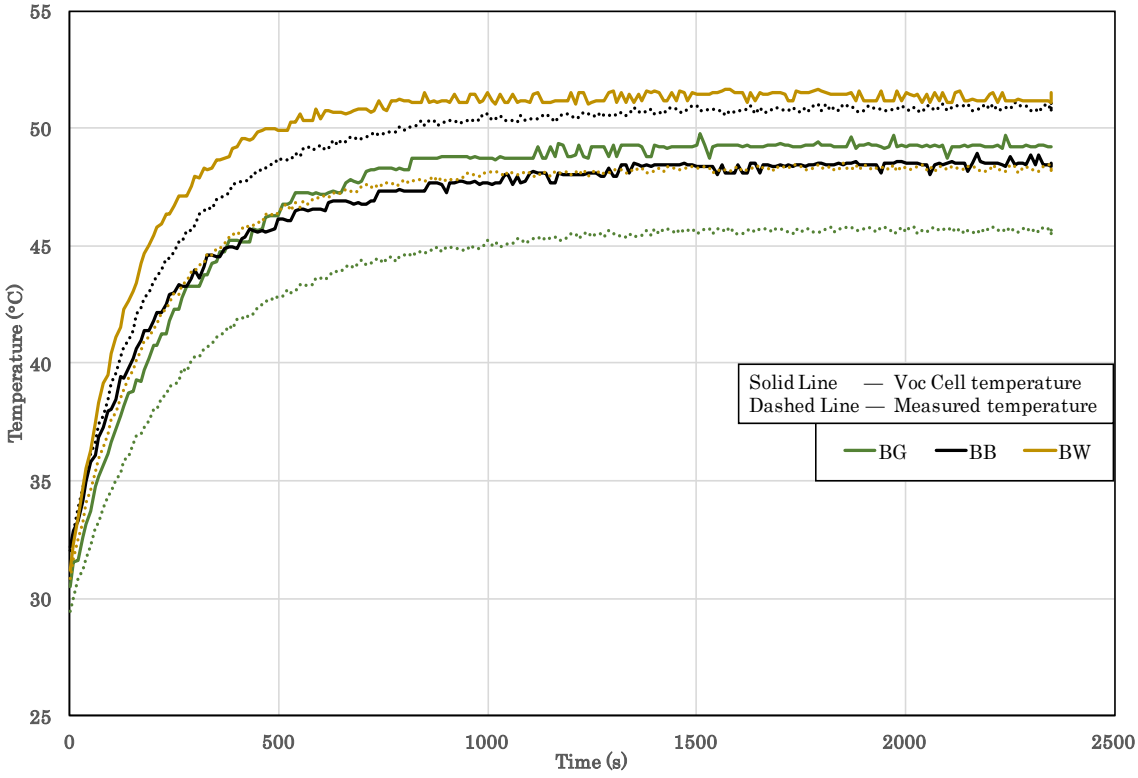

Figure 4.4 Measured and Voc cell temperatures of bifacial cell laminates

The figure 4.5 shows that the V_{OC} temperatures are higher than the measured temperatures for all the three laminates with monofacial cells. The MB laminate has the highest V_{OC} temperature which as expected due to higher absorption of the irradiance than the other two laminates. Overall, the observations from both figures gives that the V_{OC} temperature of the MB has highest temperature. In conclusion, the measured temperatures may not be best representation of the operating cell temperature as it is a measurement of backsheet (measured) temperatures. Therefore, using measured temperatures it cannot exactly be said if laminates with bifacial cells have higher operating temperatures as compared to laminates with monofacial laminates since the irradiance absorbed by the backsheets is higher for laminates with bifacial cells.

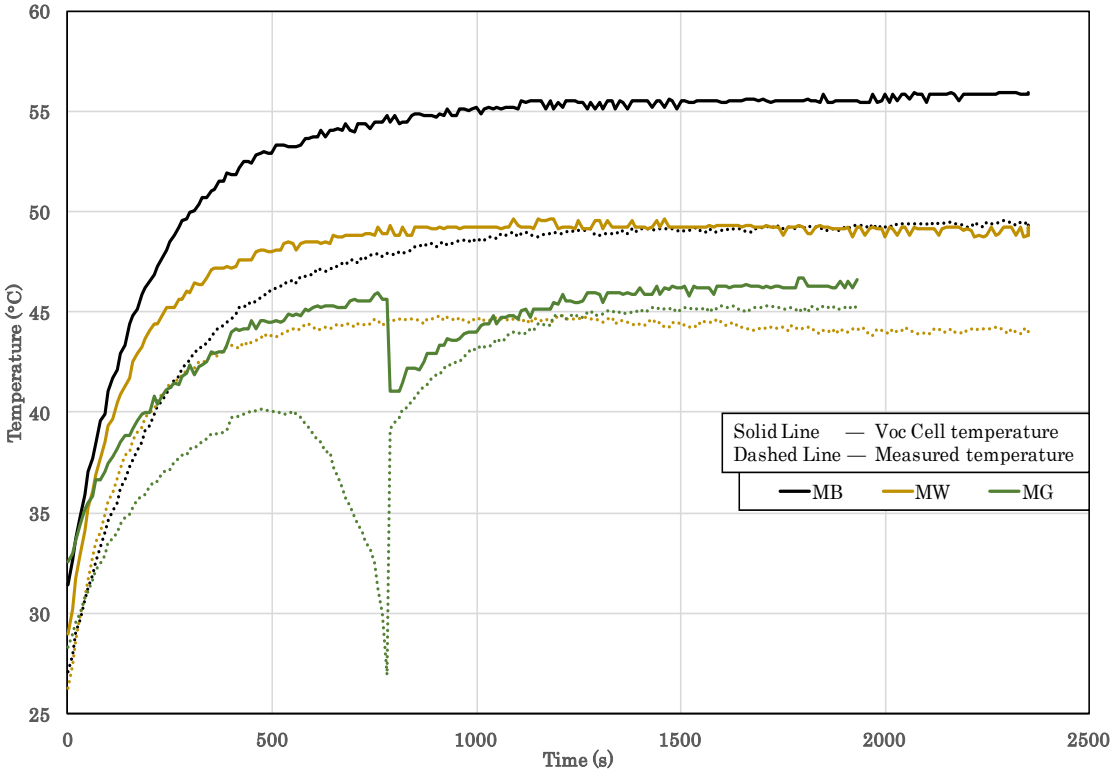

Figure 4.5 Measured and V_{OC} cell temperatures of monofacial cell laminates

The power of the solar modules is given in the figure 4.6 below. The results can confirm the expectation in terms of electrical performance of bifacial cells with different backsheets (BG, BW, BB). The white backsheet gives a high output but the black backsheet provides aesthetically suitable module. The BW laminate has 11.7 % more power than the bifacial black module. Whereas the MW laminate has 8.11 % higher power than monofacial black module. In conclusion, white bifacial (BW) laminates can be used if the high output is wanted while black bifacial (BB) laminates may be preferred for aesthetic purposes though the power output is lower than the BW laminates.

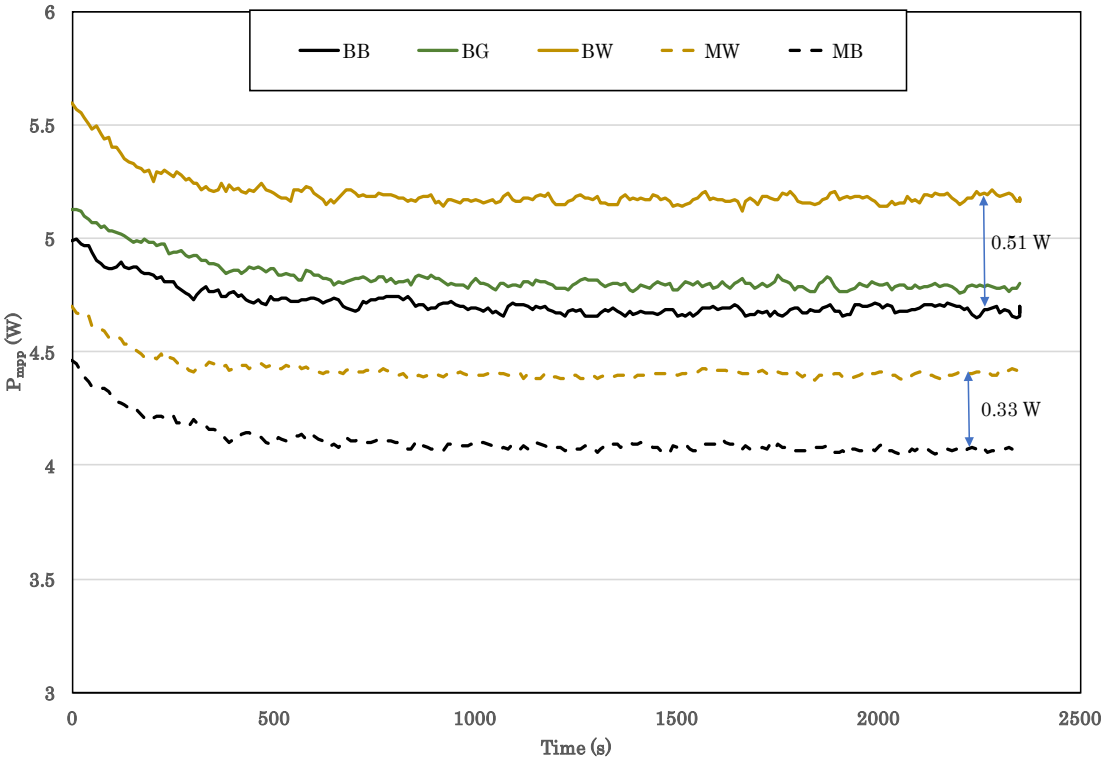

Figure 4.6 Power at maximum power point of the solar cell laminates

4.3 Modelling module temperature

The temperature behavior of the modules was modelled using the curve-fit technique. The equation for this curve fit was found to be as given in equation 4.1 which is same as the equation 2.16.

$$T_m(t) \quad = T_a + \frac{Q_{in}}{U} - \left(\frac{Q_{in}}{U} - T_a + T_o\right) \bullet e^{-\frac{U}{C_{TH}}t} \tag{4.1}$$

The three parameters heat transfer coefficient, U, heat capacity C_{TH}, and initial temperature of the laminate, T_o, in the above equation used as variables for fitting the model results with the measured results. This equation is the non-steady state model of the energy balance equation. For indoor measurements, as is the case, the inputs are constant and the temperature of the module only depends on the amount of time it is exposed to the irradiance source. Therefore, the time, t, is variable. The example of curve-fit model of energy balance equation for a glass-glass bifacial module can be seen in figure 4.7 below.

The model estimation of temperature is very close to that of the measured values. Now, this equation can be used to determine the heat transfer coefficient of the module in the environment of indoor measurements and also, the heat capacity per unit area of the module as well. In order to determine these values, the heat input and the ambient temperature values have to be considered.

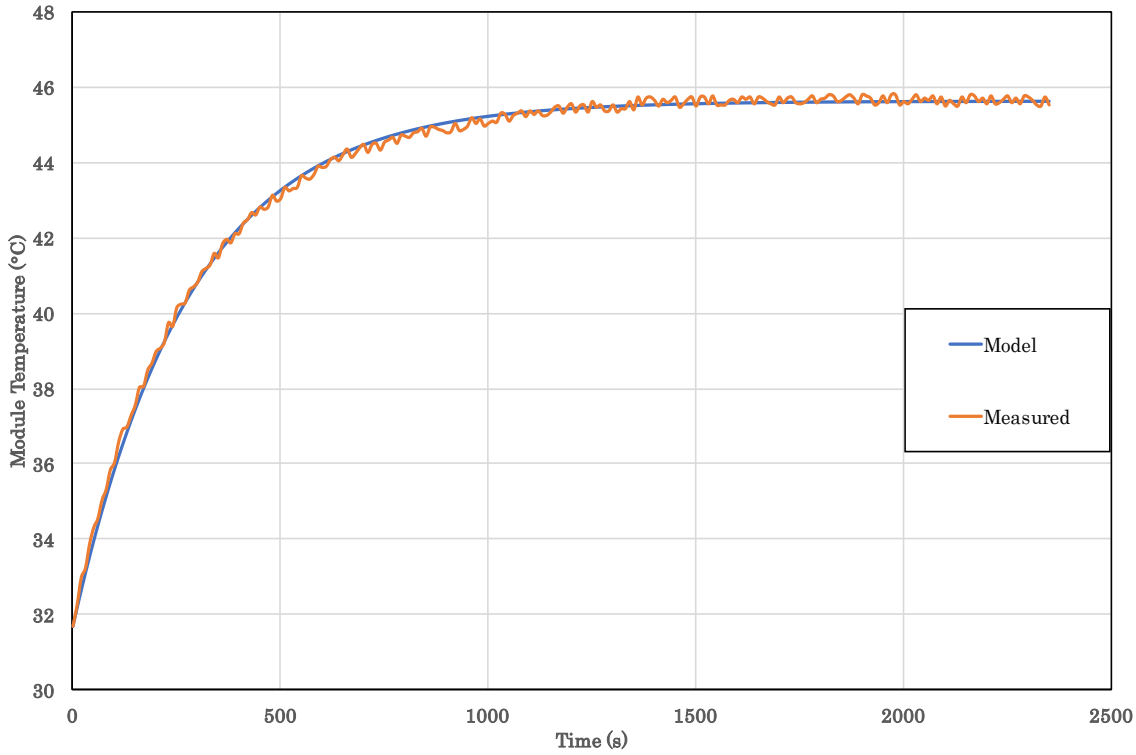

Figure 4.7 Measured and modelled temperature of bifacial glass-glass module.

Now using non-steady state energy balance equation applied to the indoor measurements, and using the curve-fit method, the values of heat transfer coefficient and heat capacity are determined and they are given in table 4.4. The heat transfer coefficient U and the heat input Q_{in} determine the steady state temperature of the laminate (or cell) as given in equation 4.2. Also, the curve fitting was applied to the V_{OC} cell temperatures as well and the values of heat transfer coefficient and heat capacity are determined and are given in table 4.5. The values of MG laminate are only approximate estimated values due to lack of good measurements.

$$Q_{in} = U(T_m - T_a) \tag{4.2}$$

Table 4.4 Heat transfer coefficient and heat capacity of six modules for measured temperature

Cell Laminate	U [W/m²•K]	C_{TH}[J/K•m²]
BG	35.3	9930
BW	33.7	6725
BB	32.1	6538
MW	43.6	5759
MB	35.5	8412
MG	32.12	9908

Table 4.5 Heat transfer coefficient and heat capacity calculated for V_{OC} cell temperature

Cell Laminate	U [W/m²•K]	C_{TH}[J/K•m²]
BG	29.73	8018
BW	30	7064
BB	35.2	8295
MW	35.76	4650
MB	28.8	4899
MG	39.4	9578

The value of the heat capacity can be applied to any environment (indoor or outdoor) as it a material property. The above calculated values of C_{TH} (table 4.4) are compared to the values calculated from the literature in table 4.7 below. The heat capacity of the module is calculated by summing the heat capacity of each layer in the module (table 4.6). The heat capacity is calculated using the equation 4.3 below and the data for the properties are obtained from literature [22] [23] [16].

$$C_{TH} = t \bullet \rho \bullet C_p \tag{4.3}$$

Table 4.6 Thermal properties of various layers of a solar module

Module Layer	t [m]	ρ [kg/m³]	C_p [J/kg•K]	C_{TH} [J/m²•K]
Glass	3×10^{-3}	2700	500	4050
EVA	450×10^{-6}	960	2090	903
PV Cell	192×10^{-6}	2300	836	370
Backsheet	350×10^{-6}	1200	1250	525

It can be observed that the value of heat capacity of the bifacial glass module is close to that of the literature data and also the other two bifacial cell laminates with backsheets have higher estimated value but it is not very irrational difference. The monofacial call laminate with white backsheet also has estimated value close to the literature data. Whereas the difference between literature and estimated values is quite large for the monofacial black module.

Table 4.7 Comparison of estimated heat capacity of six modules (for measured temperature) with literature

Cell Laminate	Literature	Estimated
BG	9903	9430
BW	5850	6725
BB	5850	6538
MW	5850	5759
MB	5850	8412
MG	9903	9578

The heat transfer coefficient values are fairly similar except for the value obtained for MG laminate but as already explained this was due to error in measurement. The conductivity of the 3 mm glass and 0.35 mm backsheet are in same order of magnitude. The observed values are in good agreement with the suggested values of PVSyst. In conclusion, the values of the heat transfer coefficient are comparable to the literature values (for indoor conditions) and the heat capacity values are also in close agreement with literature values.

5 Outdoor measurements

The setup used for the measurement is same as the setup described in chapter 3.1. The data for the whole month of June was extracted and this can be used for the comparisons with the model predictions, but only a single day (June 11th) was used for analysis. The global horizontal irradiance (GHI) and diffuse horizontal irradiance (DHI) as given in the figure 5.1 below.

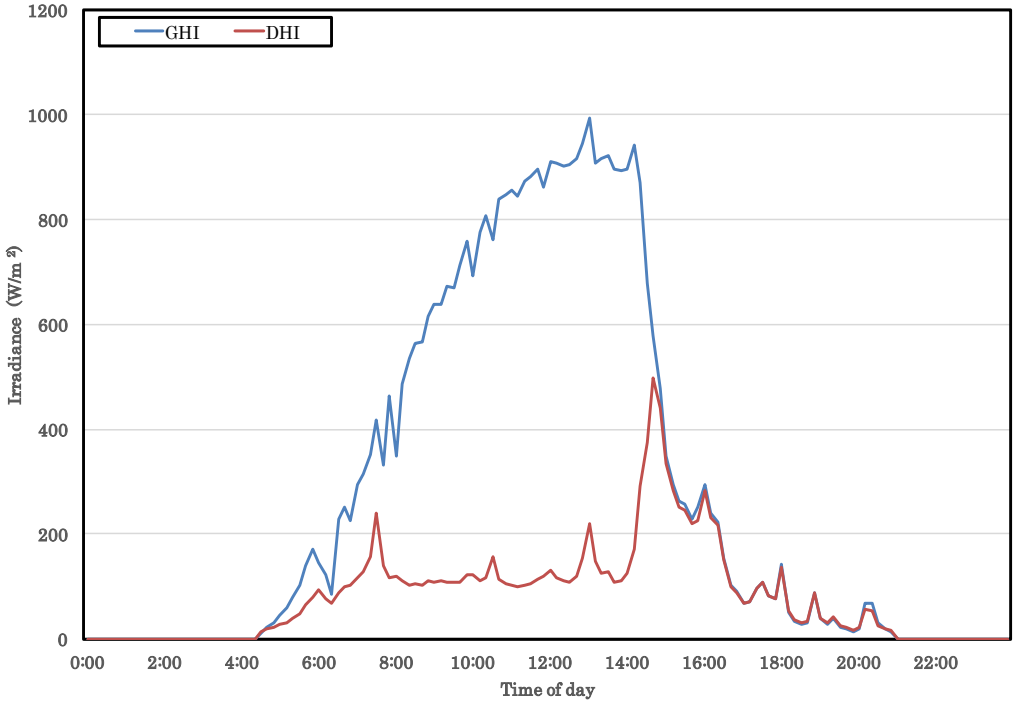

Figure 5.1 GHI and DHI of July 11th measured at the rooftop of ECN test site

5.1 Temperature analysis

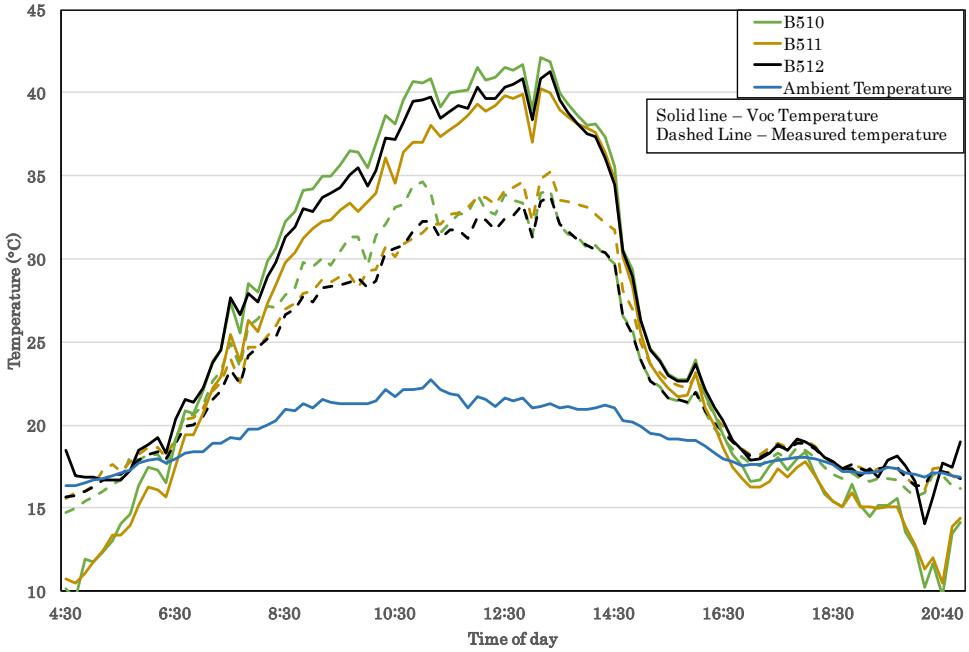

Figure 5.2 Comparison of measured and V_{OC} temperatures of the three panels

Initially the measured data of a day with good irradiance was considered (June 11th 2017) for analysis. The figure 5.1 shows the measured and cell temperatures derived from V_{OC} of the three panels. During the V_{OC} cell temperature calculation, the ideality factor was calculated using 1-diode model at the STC conditions (1000 W/m^2 and 25 °C) and therefore at low irradiances as seen at the beginning and end of the day the V_{OC} cell temperature is wrong during these periods. The reason for this could be the ideality factor is incorrect at low voltages [24].

In the indoor analysis, it was seen that the bifacial glass module had lower temperature as compared to the bifacial white module but in the figure above the difference in temperature (both measured and V_{OC}) between bifacial glass panel (B510) and bifacial white panel (B512) is low. The reason for this could be the additional absorption of irradiance on the rear side of the glass-glass panel.

The differences between the measured and V_{OC} temperatures are quite high at the middle of the day where irradiance is high as seen in figure 5.2. The difference in calculated cell temperature and module temperature at high irradiances was found to be ~6 °C. Generally, the temperature difference between cell and measured (at the back of panel) in flat plate collectors in open rack environment is about 2 °C – 2.5 °C [25]. In conclusion, the temperature of the bifacial glass panel has high temperature as much as the bifacial panel with white backsheet due to rear irradiance absorption.

5.2 Application of non-steady state model

5.2.1 Calculation of heat input, heat capacity and heat transfer coefficient

The model is applied for the bifacial glass panel. The calculation of the heat input for the panel is done using the equation 5.1. The reflectance and transmission values used for the calculation of the heat input were assumed to be same as the bifacial glass (BG) module. The efficiency measured at STC (at ECN) for the front side and calculating the rear side efficiency is used to determine the total heat input.

$$Q_{in} = \alpha_f \bullet G_f + \alpha_r \bullet G_r \tag{5.1}$$

Where the α_f and α_r are front and rear absorption factors. The thermal capacitance, C_{TH}, of the panel used here is same as the value estimated in the indoor measurements for the single cell laminates. The C_{TH} of the glass-glass bifacial module was found to be 9430 J/m^2•K from the indoor measurements. In the model, value of heat transfer coefficient used in the estimation of temperature was from the indoor measurements but in order to apply this for the outdoor conditions, the effect of wind speed has to be considered. Therefore, the equation 5.2 was derived which is the non-steady state energy balance equation. This equation is used to predict the temperature of the panel. The Δt being the time interval between two input measurement data point and during this time the input data is assumed to be constant.

$$T_m = T_a + \frac{Q_{in}}{U} + \left(T_{m\text{-}1} - T_a - \frac{Q_{in}}{U}\right) \bullet e^{-\frac{U}{C_p}\Delta t} \tag{5.2}$$

During the application of model, the heat transfer coefficient would be assumed as constant for the temperature predictions as the variations are not very high for most of the day as seen in figure 5.3. The figure shows the variation in the heat transfer coefficient values for measured and V_{OC} temperatures which are calculated based on the steady state energy balance equation 4.2.

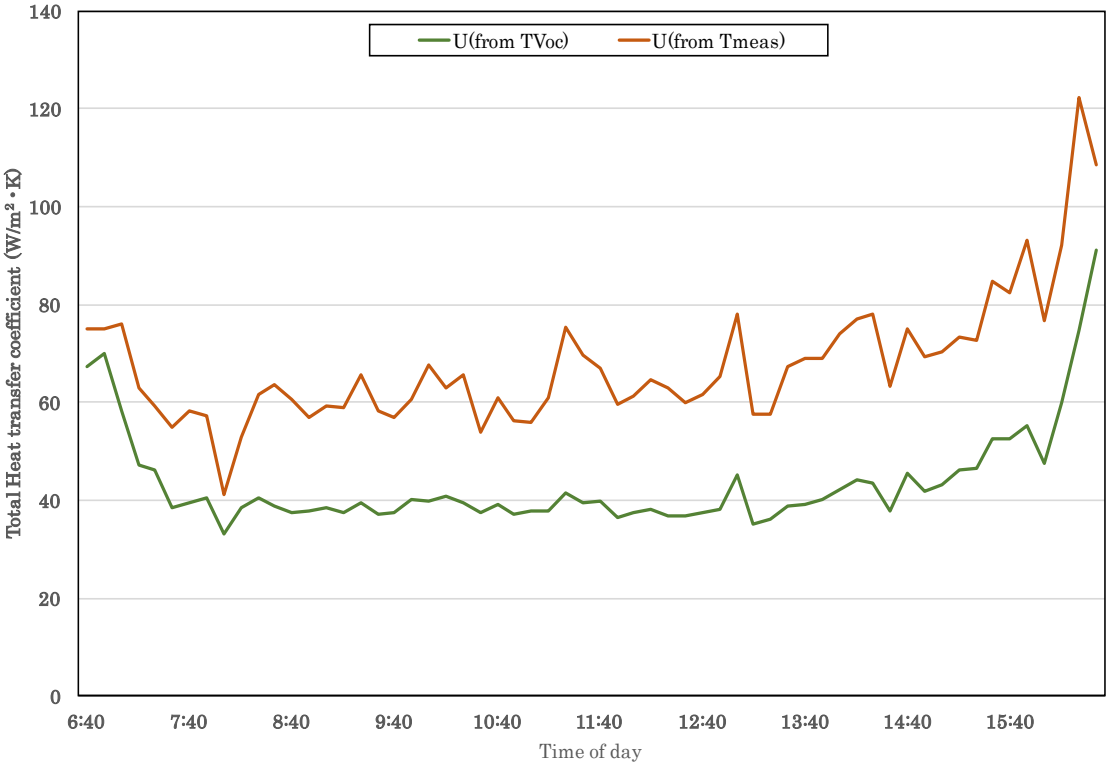

Figure 5.3 Variation of heat transfer coefficient throughout the day

Using the non-steady model for the outdoor measurements, assuming a constant heat transfer coefficient value the temperature was modelled. Using curve-fit method, the average U was estimated as it was done in indoor measurement. In order to incorporate the effect of wind speed in the heat transfer coefficient, the equation described in the PVSyst literature is utilised [18], which is also used in the ECN model. For the same day, the heat transfer coefficient values are estimated for the equation 5.3. The values for with and without wind speed are given in the table 5.3.

$$U = U_c + U_v \bullet v \tag{5.3}$$

The estimated values for the U_c and U_v are found to be 33 W/m²•K and 3.3 W/m³•K•s. respectively. Using these values, the average U for the single day (June 11th) is found to be 58.2 W/m²•K. In the figure 5.4 the estimated model temperature, measured and Voc temperature are seen. In order to match the estimated model temperature with the Voc temperature, U_c and U_v values are found to be 24 W/m²•K and 1.5 W/m³•K•s. The average value of U for the single day (June 11th) is found to be 36.2 W/m²•K.

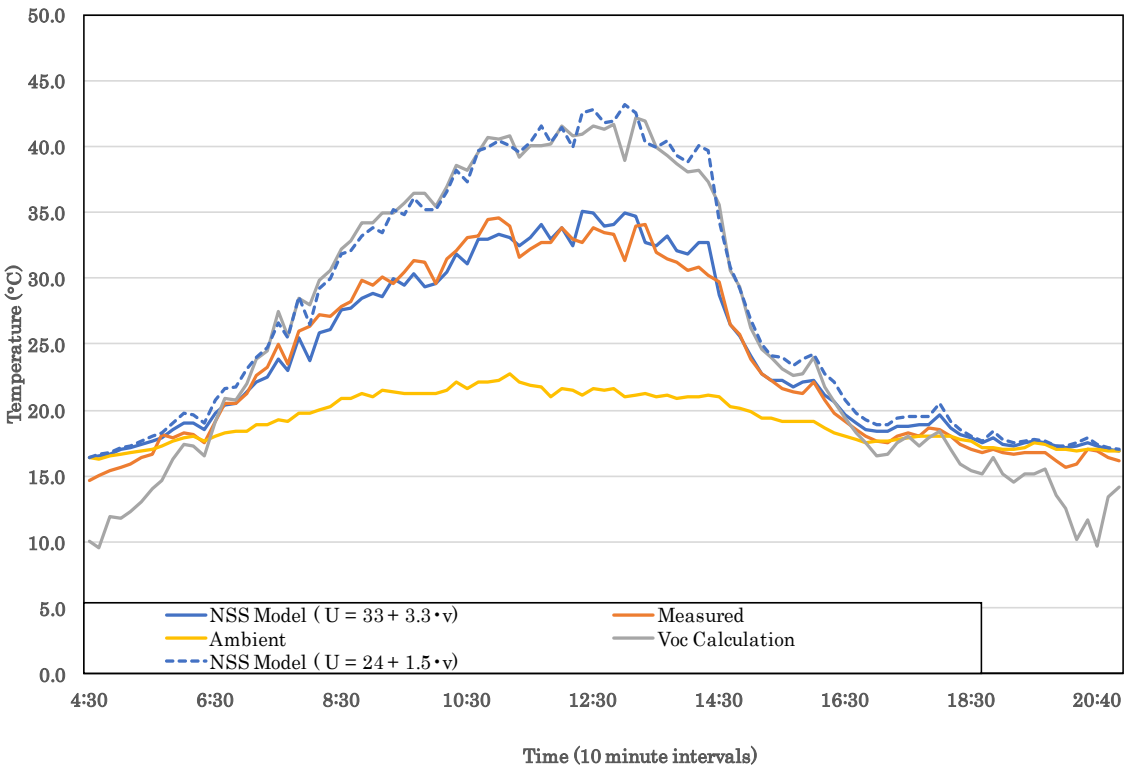

Figure 5.4 Estimated module temperature for two different U values in comparison with measured and calculated temperatures for July 11th

From the figure, the heat transfer coefficient values for Voc cell temperature are in good agreement with the PVSyst defined values from section 2.3 and the temperature measured using the PT100 sensor on the rear side of the panel may not be the best indication of the operating cell temperature.

5.2.2 Non-steady state model vs Steady state model

In this section, the temperature prediction using the NSS model is compared to the steady state model used by ECN. From the indoor measurement results, it can be seen that solar module reaches steady state value of temperature in around ten minutes. This is assuming the heat input and weather conditions as constant. Now, the data measured at ECN test site is of 10-minute interval and consider one such interval from 7:20 AM to 7:30 AM on July 11th (data of same day is used in above results). Now, dividing this one interval of 10 minutes into five two-minute intervals and assuming that for both models, the initial temperature is same as seen in figure 5.5, and heat transfer coefficient value are constant during this ten minutes. Under these experimental conditions, the irradiance is assumed to vary every two minutes.

The figure 5.5 shows the temperature of the panel as predicted by the two models. In the figure the solid line shows the temperature prediction for 12 % variation in irradiance with respect to initial irradiance and the dashed shows the temperature prediction for 25 % variation in irradiance. This is done in order to see the difference in temperature prediction between the two models for irradiance variation.

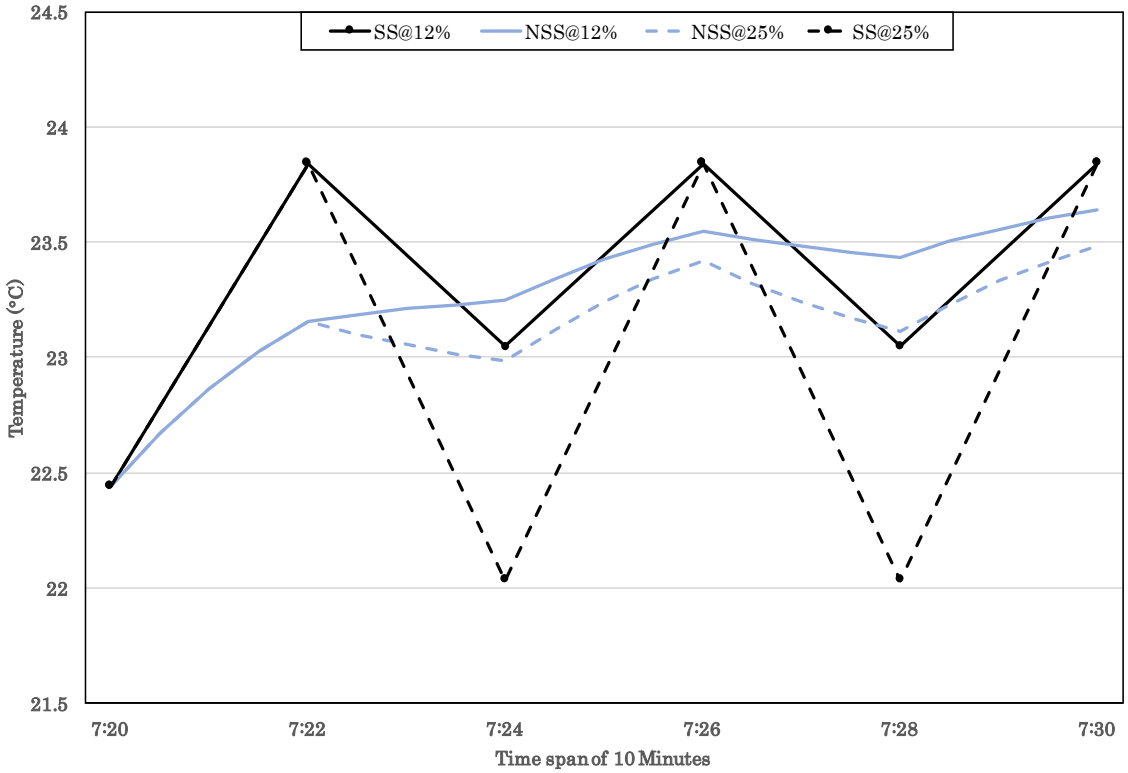

Figure 5.5 Comparison of ECN model and NSS model panel temperature predictions

From this comparison, it can be concluded that the for the meteorological data available at 1 minute and two minute intervals, the non-steady state model can be used for temperature prediction and also, if the data available for temperature model is of 10-minute or more resolution, the non-steady state model behaves as the steady state model. Though the steady state model is good enough for greater than 10-minute resolution. For the data of less than 10-minute resolution, the non-steady state model should be used. Furthermore, the non-steady model uses the panel properties which can be different for different panels based on the materials used. Also, the fact that the non-steady state model takes the previous module temperature into account, making it 'history dependent'. Therefore, it is one of the recommendation to use this non-steady state model instead of steady state model for temperature prediction and it is convenient to apply in the ECN yield model.

Using the NSS model for the hourly data is essentially same as using the steady state model. As shown in figure 5.6 the temperature prediction using steady state model from ECN and NSS model is essentially same (orange curve overlapping the blue curve) for meteorological data of 10-minute resolution. Also, the time taken by the solar panel to reach steady state temperature is dependent on the heat transfer coefficient as well, therefore it is important to consider the changing value of heat transfer coefficient due to variable wind speed. Though the effect of changing heat transfer coefficient is higher on the steady state value than on the steady state temperature than on the time taken by the panel to reach steady state.

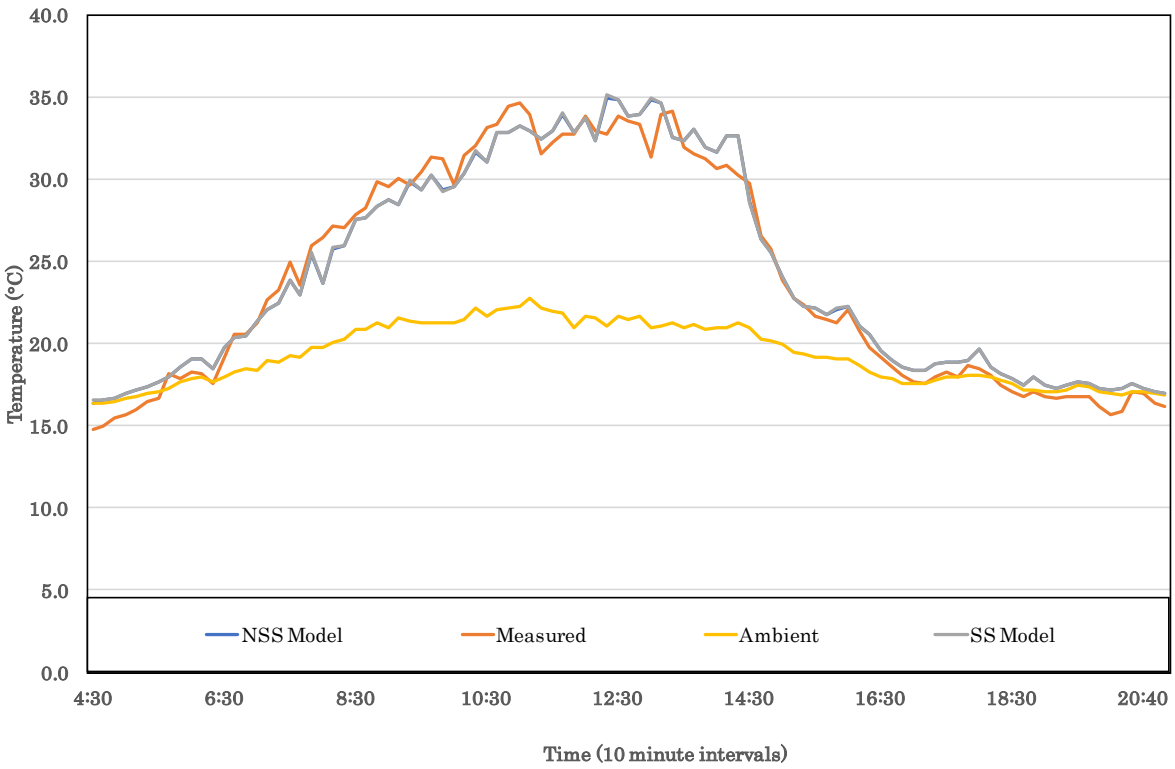

Figure 5.6 Non-steady state temperature model prediction for 10-minute interval data

The NSS model behaves as the steady state model once the time step resolution of the data exceeds or equals the time taken by the panel to reach steady state temperature which is normally around 10 minutes.

5.3 Energy yield simulations

As already described in the literature there are many models to estimate the heat transfer coefficient for solar panels which range from simple to complicated dynamic models. In this section, the effect of heat transfer coefficient on annual energy yield is simulated and the results are discussed below. Firstly, the ECN model for bifacial yield prediction was used for simulations. The model used for estimating the heat transfer coefficient is given in chapter 2. The location used for the simulation was Vassen, the Netherlands. The albedo and elevation used were 20 % and 0.5 m respectively. The tilt angle used for this simulation was 30°. The module details are given in the appendix. From previous section 5.2.1 the heat transfer coefficient was different with respect to measured and V_{OC} cell temperatures and the difference being 40 %.

The figure 5.7 shows the effect of variation in heat transfer coefficient value on the annual energy yield. It can be observed from figure 5.7 that a decrease in the heat transfer coefficient by 20 % only decreases the yield by 0.45 %. Furthermore, the decrease in heat transfer coefficient by 40 % results in a decrease in yield of 1.45 % which is a relevant reduction in power. The reduction of energy yield of 1.45 % could be a concern from financial point of view. Though in practice, there may not be a difference of 40 % in heat transfer coefficient between various models, in conclusion, it can be said that the variation in heat transfer coefficients due to its calculation using different models, has a negligible effect on the annual energy yield of a bifacial PV system. Therefore, it may not be necessary to use complicated temperature models

for estimation of yield of bifacial PV system at least for the one-hour input data resolution.

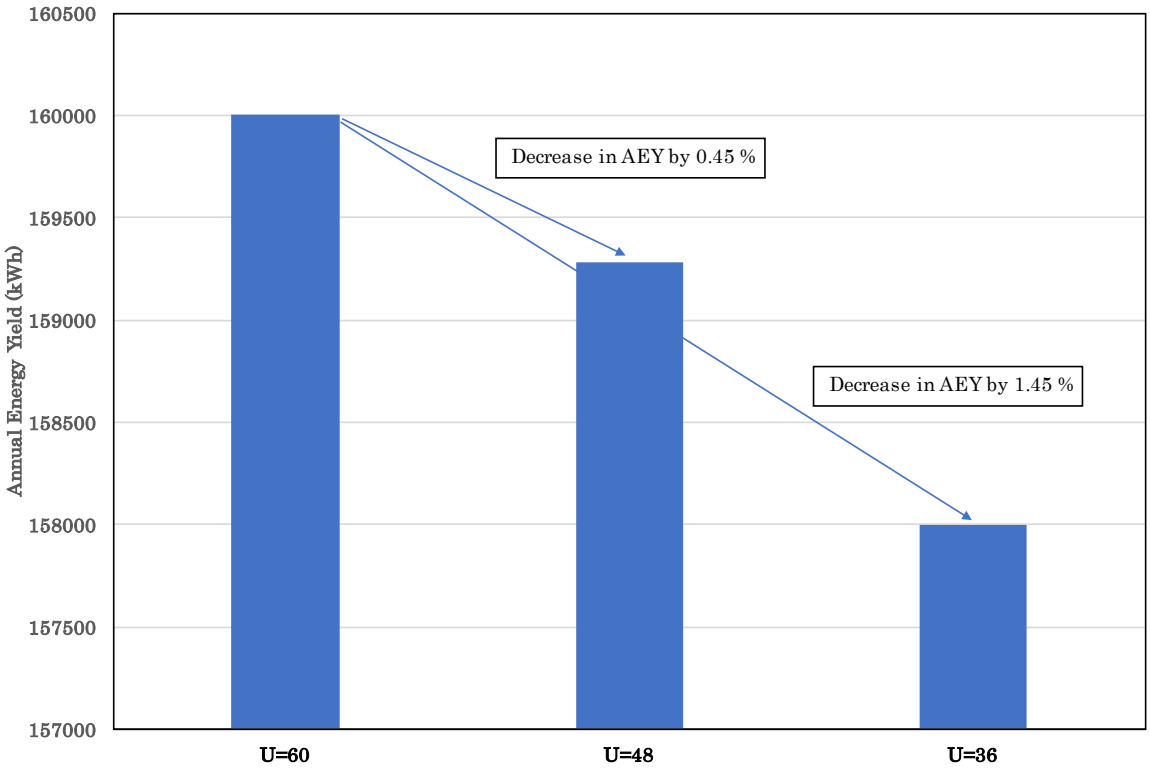

Figure 5.7 Yield variation for large system of 196 kW rated power

6 Conclusions

In order to improve the prediction of bifacial yield model developed at ECN, the objectives of the thesis as described in 1.3 were worked upon and conclusions of the work are given below.

1. During the simulation for the validation of rear irradiance for the condition when the solar panels were flat on the ground i.e. for the tilt angle of 0° and elevation of 0 m from the ground, the results indicated presence of high rear irradiance. A new factor called 'acceptance factor' was obtained from [11] and therefore incorporating this factor in rear irradiance model resulted in a very low rear irradiance for that condition.

2. After studying the view factors defined by J. Appelbaum in [12], it was more reasonable to use one single view factor (α) and compared the two separate angles used in ECN model. Furthermore, the equation 2.12 given by [12] as well, was used to implement the effect of elevation on view factor of panel to ground on the rear side. As seen in section 3.1 (figure 3.4) the increasing elevation results in increased view factor and ground acceptance and therefore higher reflected irradiance on rear. The model is validated with the outdoor data for a single day and the predicted irradiance is quite close to the measured irradiance.

3. The Indoor temperature experiment the heating behavior and its effect on electrical parameters of six different solar modules were obtained. The temperature measurement of laminates with bifacial cells are proportional to heat absorbed by them and though the laminates with monofacial cells absorb higher irradiance, they were measured to have lower temperature as compared to the bifacial cell laminates. The cell temperatures are higher than the measured temperature for all laminates except the one with bifacial cell with black backsheet. Here, the extra irradiance absorbed by the backsheet in the inactive area could have resulted in higher temperature of the backsheet than the cell itself. Also, the measured temperatures for bifacial cell laminates is higher than the monofacial cell laminates which could be due to the measurement of temperature at the backsheet and this is influenced by the extra irradiance absorbed in backsheets of bifacial cell laminates due their higher transmission. Also, the extra irradiance absorbed by the backsheet in the inactive area influences the measured temperature. The power output of the laminates with white backsheet is higher than black backsheets as expected due to the higher reflected irradiance by white backsheet.

4. The modelling of the temperature behavior was done and the using the curve-fit technique the heat transfer coefficient and heat capacity values were calculated. The results were found to be in approximate agreement with the literature values.

5. The Non-steady state temperature model that was applied to outdoor solar panels (glass-glass bifacial panel) to predict the heat transfer coefficient for outdoor conditions. The values of heat transfer coefficient for measured and cell temperatures had differences of ~40 % and this could be due to losses in conduction through the glass and also the effect of wind in the outdoor conditions is higher than the indoor conditions. This difference of 40 % was later used in calculating its effect on energy yield for error in the temperature model of 40 %.

6. Furthermore, an experiment of the steady state model and non-steady state model resulted in better temperature prediction by NSS model when the data used is of two-minute interval and it was observed that the NSS model behaves similar to steady state model when data used is of ten-minute interval. This is because the panels reach steady state temperature in approximately ten minutes.

7. Lastly, the effect of the variation in heat transfer coefficient (as a result the temperature) on the energy yield is calculated. For a reduction in heat transfer coefficient by 40 %, the energy yield was reduced by 1.45 %. Though it may not seem to be a lot, from a financial point of view, for a large-scale system this may be of concern.

The results from the ground acceptance and view factor section show that the model has the capability of prediction better energy yield for bifacial PV systems. Also, a good indication measured and cell temperatures of laminates of monofacial cells and bifacial cells are given. Furthermore, the non-steady state model is recommended to be incorporated in the bifacial yield model for better results of module temperature. For the input data of one hour resolution, the effect of using different heat transfer coefficients (by 40 %) results in low variation in annual energy yield hence using elaborate methods to calculate heat transfer coefficient may not have high effect on annual energy yield.

7 Future work

The thesis gives out results that can be further studied. The recommendations for the work that be done in the future is given below.

1. The rear irradiance model can be further validated with the measured values for a large scale bifacial PV system. Also, the validation of rear irradiance model can be done for a whole year as compared to a single day.

2. Indoor measurements can be done with the presence of controlled wind source in order see the effect of wind speed on the cell and measured temperatures of the laminates. Furthermore, an artificial albedo can be introduced on the ground to see the contribution to module temperature in the bifacial modules. Also, further measurement need to be done to understand more about the temperature of bifacial laminates as compared to the monofacial laminates.

3. The non-steady state temperature model could be compared with the other elaborate temperature models such the fluid dynamic model [13] to see the differences in temperature prediction and this can be for various input data resolution of one minute, ten minutes and 1 hour.

4. The non-steady state temperature model should be validated with the measured values of temperature at low input data resolution of one minute interval or less.

5. Lastly, a lot of work can be done regarding optimization of bifacial PV systems based on their location globally in order to get highest possible energy yield for that particular location which can be done using the bifacial energy yield model.

8 Bibliography

[1] "European Comission : Climate Action," [Online]. Available: https://ec.europa.eu/clima/policies/international/negotiations/paris_en. [Accessed October 2017].

[2] IRENA, "REthinking Energy 2017 : Accelerating the global energy transformation," International Renewable Agency, Abu Dabhi, 2017.

[3] Electric Power Research Institute, "Bifacial Solar Photovoltaic modules," Palo Alto, 2016.

[4] J. A. Coakley, "Reflectance and Albedo, Surface," 2003. [Online]. Available: http://www.curry.eas.gatech.edu/Courses/6140/ency/Chapter9/Ency_Atmos/Reflectance_Albedo_Surface.pdf. [Accessed November 2017].

[5] M. Chiodetti, "Bifacial PV plants: performance model development and optimization of their configuration," 2015.

[6] I. Shoukry, J. Libal, R. Kopecek, E. Wefringhaus and J. Werener, "Modelling of bifacial gain for stand-alone and in-field installed PV modules," *Energy Procedia,* vol. 92, pp. 600-608, 2016.

[7] G. J. Janssen, B. B. Van Aken, A. J. Carr and A. A. Mewe, "Outdoor performance of bifacial modules by measurements and modelling," *Energy Procedia,* vol. 77, pp. 364-373, 2015.

[8] J. A. Duffie and W. A. Beckman, Solar Engineering of Thermal Processes, John Wiley & Sons, 1974, p. 64 – 107.

[9] M. Chiodetti, A. Lindsay, P. Dupeyrat, D. Binesti, E. Lutun, K. Radouane and S. Mousel, "PV BIFACIAL YIELD SIMULATION WITH A VARIABLE ALBEDO MODEL," in *32nd European Photovoltaic Solar Energy Conference and Exhibition*, 2016.

[10] U. A. Yusufoglu, T. M. Pletzer, L. J. Koduvelikulathu, C. Comparotto, R. Kopecek and H. Kurz, "Analysis of the Annual Performance of Bifacial Modules and Optimization Methods," *IEEE Journal of Photovoltaics,* vol. 5, no. 1, p. 320–328, January 2015.

[11] A. Mermoud and B. Wittmer, *PVSyst new framework to simulate bifacial systems,* Freiburg: PVSyst, 2016.

[12] J. Appelbaum, "Current mismatch in PV panels resulting from different location of cells in the panel," *Solar Energy,* vol. 126, pp. 264-275, 2016.

[13] A. Smets, K. Jäger, O. Isabella, R. Van Swaaij and M. Zeeman, Solar Energy : The Physics and Engineering of Photovoltaic Conversion, Technologies and Systems, Cambridge: UIT Cambridge, 2016, pp. 437-444.

[14] M. A. Green, Solar Cells : Operating Principles, technology and system applications, Prentice-Hall, 1998, pp. 91-98.

[15] H. V. d. Akker and R. F. Mudde, Transport Phenomena : The Art of Balancing, Delft: Delft Academic Press, 2014.

[16] P. Hoang, V. Bourdin, Q. Liu, G. Caruso and V. Archambault, "Coupling opticalandthermalmodelstoaccuratelypredictPVpanel electricity production," *Solar cells and Solar materials,* vol. 125, pp. 325-328, 2014.

[17] A. Jakhrani, A. Othman, A. Rigit and S. Samo, "Comparison of Solar Photovoltaic Module Temperature Models," *World Applied Sciences Journal,* 2011.

[18] PVSyst, "PVSyst 6 Help : Array Thermal losses," [Online]. Available: http://files.pvsyst.com/help/thermal_loss.htm. [Accessed October 2017].

[19] D. Faiman, "Assessing the outdoor operating temperature of photovoltaic modules," *Progress in Photovoltaics,* vol. 16, no. 4, pp. 307-315, 2008.

[20] Eternal Sun, "Products: Solar Simulator," Eternal Sun, [Online]. Available: http://www.eternalsun.com/products/solar-simulator/. [Accessed October 2017].

[21] B. B. Van Aken, L. A. Okel, J. Liu, S. L. Luxembourg and J. A. Van Roosmalen, "White Bifacial Modules – Improved STC Performance Combined with Bifacial Energy Yield," in *European PV Solar energy Conference and Exhibition EU PVSEC*, Munich, Germany, 2016.

[22] Y. Du, W. Tao, Y. Liu, J. Jiang and H. Huang, "Heat transfer modeling and temperature experiments of crystalline silicon photovoltaic modules," *Solar Energy,* vol. 146, pp. 257-263.

[23] S. Armstrong and W. Hurley, "A thermal model for photovoltaic panels under varying atmospheric conditions," *Applied Thermal Engineering,* vol. 30, pp. 1488-1495, 2010.

[24] C. Honsberg and S. Bowden, "Measuring Ideality factor," [Online]. Available: http://www.pveducation.org/pvcdrom/characterisation/measurement-of-ideality-factor. [Accessed November 2017].

[25] D. King, W. Boyson and J. Kratochvill, “Photovoltaic Array Performance Model,” Sandia National Laboratories, 2004.

[26] B. J.T., “Materials That Absorb & Reflect Solar Energy,” [Online]. Available: http://education.seattlepi.com/materials-absorb-reflect-solar-energy-6797.html. [Accessed November 2017].